Journal of the Association for Research in Otolaryngology
https://doi.org/10.1007/s10162-025-01020-0

JARO

ORIGINAL ARTICLE

Effects of Electrode Position on Vestibular Implant Performance in Rhesus Macaque

Brian J. Morris[1] · Katherine N. Mueller[1] · Celia C. Fernandez Brillet[1] · Dale C. Roberts[2] · Roland Hessler[3] · Kathleen E. Cullen[1,2,4] · Charles C. Della Santina[1,2]

Received: 15 April 2025 / Accepted: 12 November 2025

Abstract

Purpose Vestibular implants that target the three semicircular canal branches of the vestibular nerve can partially restore the 3-dimensional vestibulo-ocular reflex (3D VOR) in individuals disabled by bilateral vestibular hypofunction. A key goal of implant design is optimizing the number, spacing, and placement of stimulating and return electrodes to maximize response strength and selectivity. While computational models provide initial insights, empirical data are essential to validate performance.

Methods We unilaterally implanted stimulating electrodes in each semicircular canal and positioned return electrodes both inside the labyrinth and outside the temporal bone in three female rhesus macaques. Using mixed-effects ANOVA, we quantified how electrode location influenced 3D VOR response magnitude and misalignment.

Results We found that: (1) the deepest stimulating electrode in each canal generally yielded the strongest and most aligned responses; (2) a 600–750 µm difference in electrode position significantly impacted VOR outcomes; (3) return electrodes placed inside the labyrinth produced significantly larger VOR responses than those placed outside the temporal bone when stimulus current is constrained to levels that elicit no sign of facial nerve excitation; and (4) "near-bipolar" stimulation—using a return electrode in the same ampulla as the stimulating electrode—yielded better alignment.

Conclusion Although including multiple stimulating electrodes per canal may lower the risk of missing the target, a VI limited to one deep stimulating electrode per canal and one common return electrode can suffice if array design and surgical technique ensure placement near the crista ampullaris. Unused stimulator channels could be repurposed in designs intended to stimulate the utricle, saccule and/or cochlea. Moreover, spatial selectivity is improved by placing return electrodes within the labyrinth or ampullae, rather than outside the temporal bone. VIs that use a single common return electrode shared by all stimulation channels could achieve better performance in the future by incorporating multiple independent return electrode channels to permit near-bipolar stimulation.

Keywords Vestibular implant · Vestibular prosthesis · Vestibular · Electrodes · Vestibulo-ocular reflex · Semicircular canal · Bilateral vestibular hypofunction · Bilateral vestibulopathy · Cochlear implant · Rhesus · Macaque · Monkey

Introduction

Bilateral vestibular hypofunction (BVH) can be caused by ototoxic drugs, genetic mutations, or other injuries to the inner ear. Also called bilateral vestibulopathy, it affects an estimated 64,000 adults in the U.S. and 1.8 million adults worldwide [1]. Affected individuals suffer chronic oscillopsia (blurred vision during head movements), dizziness, difficulty walking, fatigue, and increased risk of falling [2–6]. In a nationally representative sample of US adults, about 30% of those reporting symptoms consistent with severe BVH stop driving due to their symptoms,

✉ Charles C. Della Santina
cds@jhmi.edu

[1] Department of Biomedical Engineering, Johns Hopkins School of Medicine, Baltimore, MD, USA

[2] Department of Otolaryngology–Head and Neck Surgery, Johns Hopkins School of Medicine, Baltimore, MD, USA

[3] MED-EL GmbH, Innsbruck, Austria

[4] Department of Neuroscience, Johns Hopkins School of Medicine, Baltimore, MD, USA

40% report missing work due to their symptoms (average of 45 days per year), 60% avoided social activities, and 84% reported a fall within the last 5 years [1, 7]. Compared to age-adjusted norms, they reported greater psychological distress, worse quality of life and an estimated $13,000 mean annual economic burden of disease [2].

Standard of care treatment for BVH has changed little over the past century [8]. It includes vestibular rehabilitation, avoidance of vestibular suppressant medications, and use of assistive devices such as a cane or walker [9, 10]. Individuals with moderate BVH usually can recruit other sensorimotor systems, such as the cervico-ocular reflex and oculomotor smooth pursuit, to sufficiently stabilize gaze and facilitate walking. However, those compensatory strategies typically fail during quick head or body movements. Individuals with chronic BVH typically reach a plateau of compensation within about 6 months of onset and thereafter must live with chronic oscillopsia and postural instability [11, 12].

Vestibular implants (VI) are intended to partially restore vestibular sensation to individuals who gain inadequate benefit from standard of care treatment [13]. VIs currently under study in clinical trials of motion-modulated stimulation focus on semicircular canals, sensing head motion and modulating the rate and amplitude of current pulses delivered via electrodes implanted in each semicircular canal ampulla. In humans and animals, VI stimulation can drive the vestibulo-ocular reflex (VOR), eliciting eye movement responses that approximately align with the targeted canal's anatomic axis [14, 15]. Human VI recipients followed for 0.5–5 years post-implantation while receiving continuously motion-modulated stimulation experienced improvements in dizziness, quality of life, posture and gait [16]. However, despite those successes, room remains to further optimize surgical technique, electrode design, and electrode positioning.

Because VI electrodes are typically surrounded by electrically conductive inner ear fluid and tissue, current spread away from stimulating electrodes reduces the strength and selectivity of VI stimulation, driving less activity in the targeted nerve branch while inadvertently activating non-target vestibular nerve branches, the cochlear nerve and the facial nerve. Device designers must therefore simultaneously address multiple constraints. An electrode too far from its target (e.g., primary vestibular afferent neurons in a crista ampullaris) may fail to excite the target neurons with sufficient intensity, resulting in weak eye movement responses with low velocity even at high stimulus currents. An electrode too near non-target neurons will inadvertently stimulate them, eliciting a distorted head motion percept (if the wrong vestibular afferent neurons are activated), tinnitus (via excitation of cochlear neurons) or facial twitching (if current spreads to the facial nerve). In practice, those non-target effects reduce VI performance by constraining the range of current levels available for stimulating targeted neurons.

Intuitively, the ideal location for an intra-ampullary stimulating electrode is immediately adjacent to the base of that canal's crista ampullaris (which for this report we define as the point where the center of that canal's ampullary nerve leaves bone and enters the crista). Histologic examination of rhesus monkeys implanted with VI arrays simulating those used in humans shows that this can be achieved [17]. However, the crista is a small target – its height (from the base of the crista to the midpoint of its connection with the cupula), width (along the local direction of endolymph flow during head rotation) and breadth are about 340 µm, 190 µm and 920 µm, respectively – and over-insertion by ~ 100–200 µm could damage or even shear off the crista, while deliberately under-inserting to avoid that error could result in poor stimulation efficacy and selectively [18]. Few published data are available to guide the optimal design of VI electrode arrays and surgical technique [17–19].

The ideal location for a return electrode is even less clear. Typically, as the distance between the stimulating and return electrodes decreases, the current field becomes more compact and spatially selective. Thus, it follows that a "monopolar" arrangement with the return electrode outside the temporal bone should yield more intense and less selective stimulation than a "bipolar" stimulation paradigm with the return electrode inside the labyrinth. Our experience with human VI recipients is consistent with this proposal: those with a return electrode outside the temporal bone (*distant return*) generally have measurable VOR responses at lower threshold currents but also experience tinnitus or facial twitch at lower currents and exhibit usually greater VOR misalignment compared to responses elicited using a return electrode near the common crus (CC, junction between the anterior and posterior semicircular canals) or elsewhere in the labyrinth (*labyrinth return*) [14, 15]. Whether the larger responses and lower excitation threshold currents (and thus longer battery life or smaller battery size) typically achieved using a *distant return* electrode outweigh the better stimulation selectivity that might be achieved with a *labyrinth return* electrode is unclear. To guide decisions regarding further device design optimization and to guide surgeons and patients contemplating VI implantation, we need empiric evidence comparing the relative efficacy and selectivity of VI stimulation using a *distant return* electrode versus a *labyrinth return* electrode in or near the common crus.

Like the commercially available cochlear implant (CI) upon which it is based, the VI we study with human recipients has only a single common return electrode through which every ampullary stimulating electrode's current must return. It is implanted either in the labyrinth (typically in or near the common crus) or outside the temporal bone [14, 16, 20]. At least one other VI can deliver "near-bipolar"

stimulation, in which the stimulating and return electrodes are in the same ampulla; however, monopolar stimulation is most commonly used with that device because it typically yielded larger responses than near-bipolar stimulation [21]. Some other VIs currently in clinical trials are also limited to a single return electrode, unlike circuitry we have employed for VI stimulation in animals [22, 23]. To guide decisions regarding further development, the VI field needs empirical evidence on the relative efficacy and selectivity of near-bipolar (*ampullary return*) stimulation compared to a shared *labyrinth return* and "monopolar" (a shared *distant return*) stimulation.

Relationships between electrode position, VOR magnitude and VOR misalignment have been explored using computational modeling. Using model geometry derived from high-resolution imaging of rodents and rhesus monkeys, finite element analysis, and computational models of action potential initiation and conduction, primary afferent neuron activity was predicted for each of the five vestibular nerve branches [18, 24, 25]. Expected VOR response axes were predicted using relative proportions of neuronal activity predicted for each of the three canals. The model predicted that a larger proportion of afferents originating in the targeted canal will be excited when using a *labyrinth* or *ampullary return* electrode (using an electrode within the ampulla of the stimulating electrode as a return electrode) as opposed to a *distant return*. Consistent with intuition, modeling also suggested that deeper ampullary stimulating electrodes should outperform electrodes further from the crista.

The goal of the present study was to measure how VI stimulating and return electrode positioning affects prosthetically evoked VOR magnitude and misalignment in the nonhuman primate labyrinth. We unilaterally implanted three rhesus monkeys with electrode arrays that each included three or four electrodes per ampulla, at least one *labyrinth return* electrode, and a *distant return* electrode. We recorded 3-dimensional (3D) VOR responses of alert, chronically implanted animals using scleral coil oculography in response to prosthetic electrical stimuli using a large set of stimulating and return electrode combinations while systematically increasing current amplitude for biphasic, symmetric, charge-balanced constant pulses. We compared physiologic data to the location of each electrode determined by high-resolution CT scans.

Methods

Overview

Three adult female rhesus monkeys (*Macaca mulatta*, Monkeys N [RhF73AN], O [RhF80CO], and G [RhF60738G]) were studied in these experiments, which were conducted under a protocol approved by the Johns Hopkins Animal Care and Use Committee, accredited by the Association for the Assessment and Accreditation of Laboratory Animal Care (AAALAC) International.

Each animal was implanted with a head cap and scleral magnetic search coils to record 3D angular eye position. After recovery from coil implantation, VOR responses were measured during whole-body sinusoidal rotation in darkness to confirm the normal function of the vestibular, oculomotor and eye movement measurement systems. Each animal was then unilaterally implanted with an electrode array in the left labyrinth. With the animal's head fixed in darkness, we then delivered biphasic, charge-balanced, symmetric current pulses (cathodic-first at the stimulating electrode, anodic-first at the return electrode) through a percutaneous connector while recording electrically evoked VOR (eeVOR) responses.

Head Cap and Eye Coil Implantation

Under sterile conditions and general inhalation anesthesia (1.5–5% isoflurane), titanium screws and poly(methyl methacrylate) dental acrylic (Lang Dental, Wheeling, IL) were used to rigidly fix a cylindrical enclosure made from poly(ether ether ketone) to the cranium. Two search coils were implanted under the conjunctiva and sutured to the sclera of one eye for each animal (left eye for Monkey G and right eye for Monkeys N and O). One coil encircled the iris; the other was superolateral and approximately perpendicular to the first. Each 5–7 turn coil's two perfluoroalkoxy-coated steel wire leads were tightly twisted and tunneled subcutaneously to the enclosure.

Motion Stimuli

To confirm the implanted search coils and recording system were working as expected, eye movement responses were measured at 1 Hz sinusoidal 100°/s peak velocity during whole-body yaw rotation of alert animals in light using an Earth-vertical-axis rotator with the animal upright and its left horizontal canal axis approximately aligned with the rotator's axis.

Eye Movement Measurement and Analysis

3D angular eye position of alert animals was recorded in darkness. A cuboidal frame around the animal's head comprised three pairs of single-turn metal coils generating three mutually orthogonal magnetic fields encompassing the animal's head. Field-generating coils coaxial with the animal's nasooccipital (X, + nasal), interaural (Y, + left) or superoinferior (Z, + superior) directions oscillated at 79.4, 52.6 and 40 kHz respectively, inducing a time-varying voltage in each

implanted coil that after demodulation yielded three voltages proportional to the angles between that coil and each field coil axis. Demodulated signals were passed through a bank of analog eight-pole, 100 Hz corner frequency low-pass Butterworth filters before simultaneous sampling at 1 kHz and recording via a data acquisition interface (Cambridge Electronic Design Power1401-3 running Spike2 software).

We used 3D rotational kinematics to orthogonalize raw data streams from the two scleral coils and compute eye angular position in the field-generating coil's frame of reference; smoothed those data using a Savitzky-Golay polynomial filter; and then computed eye angular velocity components about each implanted semicircular canal [26]. To derive individualized rotation matrices that transform angular velocity data from head (and field coil frame) coordinates to canal coordinates, we used multiplanar reconstructions of each animal's CT image data to define stereotactic planes of the skull relative to the field coil frame and relative to three mutually orthogonal planes approximately aligned with the implanted ear's semicircular canals. Because each canal in the implanted labyrinth was approximately parallel to its complementary canal in the opposite ear, we refer to those axes as the left-anterior/right-posterior (LARP), right-anterior/left-posterior (RALP), and left-horizontal/right-horizontal (LHRH) canal axes. To facilitate comparison between eye movement responses and prosthetic stimuli, we defined the head's + Z axis (positive superior) to be equal to the + LHRH axis and therefore perpendicular to the mean horizontal canal plane, which in rhesus monkeys is pitched ~ 15° nose-up from the stereotactic horizontal plane traditionally fit to the interaural axis and cephalic edges of the infraorbital rims, as illustrated in Fig. 1 [27, 28]. The head + Y (positive left) axis is the interaural axis. The head + X (positive anterior) is perpendicular to + Y and + Z. The canal-aligned + LARP, + RALP axes are in the head XY plane, with the + LARP axis 45° away from + X and 135° away from + Y; and the + RALP axis is 45° away from both + X and + Y.

We used a right-hand rule convention to specify rotation polarity (Fig. 1). For an eye that starts in a resting position, with the animal upright and looking straight ahead along the head's + X (nasal) axis, positive right-hand rule rotations about the head's + X (roll), + Y (pitch), and + Z (yaw) axes would, respectively, roll the eye in the YZ plane so its superior pole moves toward the right ear, pitch the eye in the XZ plane so the pupil moves *down*, and turn the eye in the XY plane so the pupil moves toward the *left* ear. From that same starting position, + LARP and + RALP eye rotations would both roll the eye's superior pole toward the right ear, but the former would pitch the eye up (moving the pupil superior) whereas the latter would pitch the eye down. For an eccentric starting eye position aligned with the + LARP axis (i.e., looking 45° to the right of midline in the plane

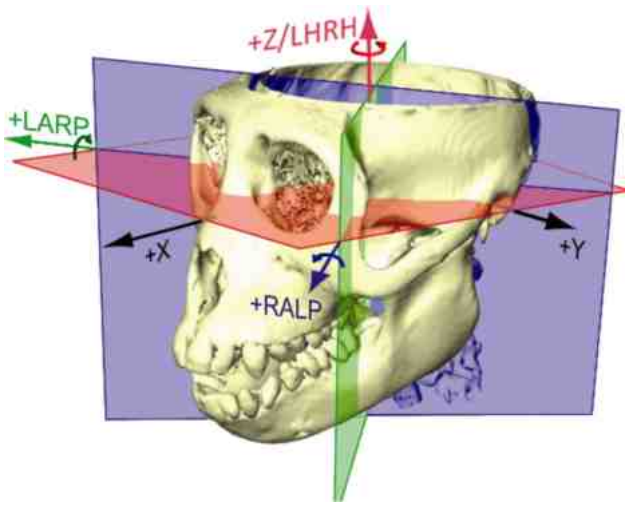

Fig. 1 Coordinate system used when analyzing vestibuloocular reflex (VOR) responses. The nasooccipital (X, + nasal), interaural (Y, + left) and superoinferior (Z, + superior) orthogonal stereotaxic axes were coaxial with the field-generating coils. 3D VOR angular position was used to calculate angular velocity in the head-fixed X/Y/Z coordinate system, which was transformed using animal-specific rotation matrices to a canal coordinate system comprising left anterior-right posterior (LARP), right anterior-left posterior (RALP) and left horizontal-right horizontal (LHRH) axes. Reprinted from Dai et al. (2013) with permission from Springer Nature

containing + X, + Y, + LARP and + RALP), a + LARP eye rotation would turn the eye about the line of sight, moving the eye's superior pole toward the right and posterior, whereas a + RALP rotation would move the pupil superior. Unfortunately, VOR physiology does not map intuitively to the right-hand rule convention used to describe 3D eye movements. Excitation of the LA, LP and LH canals normally drives slow-phase VOR responses that by the right-hand rule are, respectively, positive about + LARP and + RALP but *negative* about + LHRH (because rightward eye rotation in the horizontal canal plane is opposite the direction of a positive right-hand rule rotation about the + LHRH axis).

After decomposition into canal-aligned components, angular velocity data were smoothed using a moving average filter. For each component, the mean velocity during the 100 ms immediately before the onset of each cycle of stimulation was subtracted from responses to prosthetic stimulation measured during that stimulation trial. Cycle-averaged 3D slow-phase VOR velocity was calculated by averaging each component of eye velocity independently, at each time point, for all non-rejected cycles. Quick phases or blinks in the non-rejected cycles were excised and spline interpolation was applied. Trials were excluded if quick phases, blinks, or other large-amplitude noise existed within the 100 ms window. For the component of 3D VOR velocity aligned with the axis of the canal targeted by the prosthetic stimulation

during that trial, the time of the peak VOR relative to stimulation cycle start time was identified. At that timepoint, the values of the three VOR velocity components were extracted and used to calculate the VOR velocity magnitude for that cycle. The same three VOR component values were used as a vector to represent the axis of rotation of the eye during that cycle. The angle between the ideal VOR response (parallel or antiparallel to the targeted canal's anatomic axis in the coordinate system shown in Fig. 1) and the 3D eye velocity response axis was computed (always yielding a positive number) to yield a scalar measure of response misalignment. Average slow-phase VOR velocity magnitude and misalignment were calculated by aggregating over all non-rejected cycles.

Electrode Array Implantation

An electrode array connected to a percutaneous connector was implanted in the left labyrinth under sterile conditions and general anesthesia through a transmastoid surgical approach described previously [14, 15, 20, 27, 29]. Electrode arrays comprised 90% platinum/10% iridium electrodes at the ends of PTFE-coated platinum-iridium wire leads embedded in silicone (Fig. 2A-E).

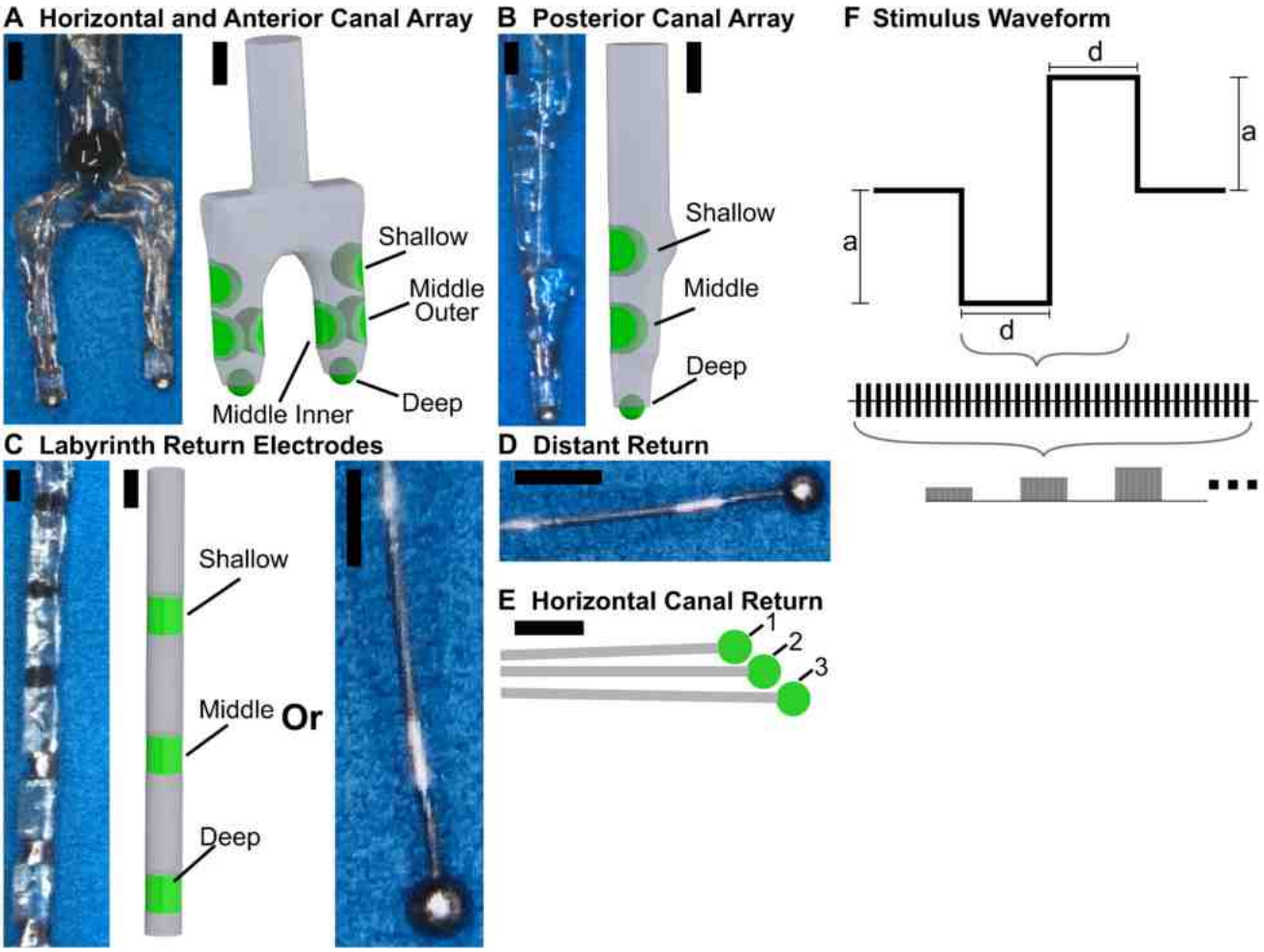

Fig. 2 Electrode arrays and stimulus waveforms. (**A**) Forked electrode array for the anterior and horizontal canals as implanted in Monkeys N and O. The electrodes on each fork of the array were spaced 600 µm center-on-center. Monkey G's array was the same except that it did not have *Middle Inner* electrodes. (**B**) The linear stimulating electrode array implanted in the posterior canal was the same for all three monkeys. The electrodes on this array were spaced 750 µm apart, center-on-center. (**C**) The linear array of three *labyrinth return* electrodes with electrodes spaced 1.5 mm center-on-center (used for Monkeys N and O) and the single ball style *labyrinth return* electrode (used for Monkey G). The three black marks in the upper half of the photo are used to measure insertion depth intraoperatively. (**D**) The *distant return* single ball style electrode implanted in the occipitalis muscle and was the same for all three monkeys. (**E**) Illustration of return electrodes implanted in Monkey O's horizontal canal. (**F**) Stimulus waveform shape and timing. The bottom row of rectangles shows blocks of pulse trains delivered with increasing current amplitude. Stimuli were delivered in pulse trains at 200 pulses/s, at current amplitudes (a) ranging from 25–250 µA, with a 0 µs interphase gap and a 200 µs phase duration (d). Black scale bars in each panel represent 500 µm

Arrays for the anterior and horizontal ampullae were joined to form a forked array, which was inserted in the anterior and horizontal canals via a pair of ampullotomies near the junction of those canals. Each shank of that fork had either 3 or 4 electrode contacts: a 300 µm diameter hemispherical ball contact *Deep* electrode; 500 × 500 µm *Middle Outer* and *Shallow* electrodes spaced 600 µm center-to-center along the surface farthest from the other shank; and (in Monkeys N and O but not G) a *Middle Inner* electrode on the subarray's surface closest to the other shank of the fork (Fig. 2A).

Each animal's posterior canal was implanted via a canalotomy near the ampulla with a single-shank linear electrode array including one *Deep* electrode at the tip and *Middle* and *Shallow* electrodes (Fig. 2B). Center-to-center spacing between adjacent electrodes on that array was 750 µm. *Labyrinth return* electrodes were inserted via a second opening in the posterior canal's thin segment and blindly advanced away from the ampulla with the intent of positioning them in the common crus. The design and final positions of those electrodes varied between animals. Monkey G had a single ball electrode in the common crus via the posterior canal. Monkeys O and N's implants each included a linear array with three 400 × 400 µm electrodes spaced 1 mm center-to-center inserted via the posterior canal (Fig. 2C). For all three animals, a *distant return* ball electrode was implanted in the occipitalis muscle outside the temporal bone (Fig. 2D). Monkey O's horizontal canal was implanted with an additional set of custom fabricated three ~ 250 µm diameter ball-type return electrodes (Fig. 2E). In addition to undergoing electrode array implantation into all three ampullae, Monkey G was also treated bilaterally with intratympanic gentamicin to ablate vestibular hair cell function [29]. Monkeys N and O were not treated with gentamicin.

Prosthetic Stimulation

With the animal alert and head-fixed in darkness, electrical stimulation was delivered via a percutaneous connector and a microcontroller controlling a Keithley 6221 current source. A microcontroller operated a cross-point analog switch able to connect any electrode as a source (stimulating electrode) or sink (return electrode). The microcontroller generated timing signals recorded by a high-speed and resolution data acquisition unit (Cambridge Electronic Design POWER1401-3) to synchronize eye movement and electrical stimulation data. Stimulation pulses were biphasic, constant-current, symmetric, cathodic-first and charge-balanced pulses delivered at 200 pulses/s, with current amplitudes ranging from 25–250 µA, a 200 µs phase duration, and a 0 µs interphase gap (Fig. 2F). For each electrode combination and current amplitude, pulses were delivered in trains by cycling stimulation on for 250 ms then off for 250 ms a total of 20 times. The maximum current amplitude tested for a given pair of stimulating and return electrodes was either 250 µA or the smallest current amplitude at which a facial twitch was first observed, whichever occurred first. We defined the maximum allowable current (MAC) as the current amplitude just below the threshold at which a facial twitch was observable (or the maximum current tested if no facial twitch was observed). The current amplitudes described above were tested for each stimulating and return electrode combination.

In addition to the *distant* or *labyrinth return* electrodes, *ampullary return* electrodes (using an electrode within the ampulla of the stimulating electrode as a return electrode) were also tested. The array of three return electrodes originally intended to be implanted in Monkey O's common crus was also used as stimulating electrodes, because two ended up in the vestibule. Those fortuitously malpositioned electrodes were tested as intravestibule stimulating electrodes and as *near-bipolar return* electrodes.

In addition to the pulse trains described above, electrical stimulation was also delivered as a 40 s duration step in the amplitude of biphasic current pulses, with a pulse amplitude of 75 µA when using a *distant return* or 250 µA when using a *near-bipolar return*, delivered at 200 pulses/s with a 200 µs phase duration and a 0 µs interphase gap. For that stimulus, which was intended to prosthetically emulate a constant-acceleration step of head rotation, the VOR response was recorded prior to the onset of stimulation and for 20 s after turning off stimulation.

To measure each stimulating electrode's impedance, we delivered 20 constant-current 100 µs/phase 100 µA biphasic pulses through that electrode and the (much larger) distant return electrode while monitoring the voltage at the output of the stimulator. From those data, we estimated the real and reactive components of impedance then computed the impedance magnitude at 5 kHz, which ranged from 5.3–14.3 kΩ. During measurements of prosthetically evoked VOR responses, the voltage across the stimulating/return electrode pair never exceeded 5.5 V, which is within the compliance voltage ranges of the current source we used during these experiments (100 V) and the Labyrinth Devices Multichannel Vestibular Implant we use in clinical trials (6.8 V). For the most intense stimuli (250 µA/phase and 200 µs/phase) and smallest electrode surface area (140 K μm^2) used during these experiments, charge injection and density per phase (0.05 µC and 36 $\mu C/cm^2$, respectively) remained within safe limits for cochlear implants defined by the ANSI/AAMI CI86:2017 standard (0.26 µC and 216 $\mu C/cm^2$) [30]. The safety of stimuli we used is further supported by the fact that VOR responses were consistently elicited over hours of stimulation for each of numerous experiments performed with each animal over > 4 months.

Statistical Analysis

Data are reported as mean ± standard error of the mean (SEM) unless noted otherwise. When comparing stimulating electrodes, the best-performing electrode was defined as the electrode that elicited the largest VOR response magnitude as averaged over all return electrodes when tested at the MAC individually defined for each stimulating-return electrode combination. (Specifically, we identified the largest VOR response that each stimulating-return electrode pair could achieve without evidence of facial nerve activation, then determined which stimulating electrode performed best when averaged over all possible return electrodes.) An analogous approach was applied when comparing return electrodes, by aggregating responses across all possible stimulating electrodes.

For the resulting multifactorial repeated-measures data sets, we used an Aligned Rank Transform (ART) analysis of variance (ANOVA) [31, 32] to compare VOR velocity or misalignment elicited by different stimulating electrodes while controlling for animal, canal and return electrode. Stimulating electrodes being compared were fixed effects in the ANOVA, while random effects canal and return electrode were both nested within animal. A similar procedure and model were used to compare the performance of return electrodes, using return electrode as a fixed effect and including stimulating electrode as a random effect. To compare return electrodes within a single animal, a similar model was implemented but without *animal* being included as a random effect. Differences were considered significant when $p < 0.05$.

Linear mixed effects models were used to quantify effects of measured electrode distance to target canal crista on VOR velocity and misalignment [33]. This analysis was performed separately for responses elicited using a *distant return* or *labyrinth return*. The models included either VOR velocity or misalignment as dependent variables, electrode distance to crista as a fixed effect, and random effects that allow variability in intercept and slope based on target canal nested within animal.

Acquisition and Segmentation of Computed Tomography Images

Computed Tomography (CT) images with 100 µm isotropic voxels were acquired with the animal under general anesthesia. Multiplanar reconstruction and 3D segmentation of the semicircular canals, cochleae and implanted electrodes were conducted using 3D Slicer. To define neural anatomy, the temporal bone of a normal rhesus macaque was scanned using 48 µm isotropic voxel micro-MRI and segmented [18]. Segmented geometry was exported from 3D Slicer to SolidWorks. The micro-MRI geometry, showing canals and cristae with high resolution, was aligned with the segmented canals from each animal's CT. SolidWorks models of electrode arrays were aligned with segmented CT electrode geometry to estimate the location of each electrode. In SolidWorks, the distance from each stimulating electrode to its target was measured along the shortest possible path within the bony labyrinth lumen, which was always a straight line for anterior and horizontal canal electrodes but curved along the canal's thin segment inner wall for some posterior canal electrodes (Fig. 3). The base of the crista ampullaris (defined above) was used as the target location. SolidWorks models of electrode arrays were accurate to within ~ 20 µm, and we estimate that electrode-target distance measurements are accurate to within ~ 10–50 µm. (Because many voxels contribute to co-registration and distance measurements, spatial accuracy and precision can be better than the minimum voxel dimension, but they depend on how well the normal labyrinth imaged using microMRI approximates the experimental animal's labyrinth and CT. In humans, semicircular canal shape, size, location, orientation and inter-canal angles vary modestly between individuals, and we expect similar variation for monkeys [34].)

In practice, electrode array engineers and implant surgeons can only control intended electrode position, not the actual position. For example, although they may intend that the "deep" electrode rests adjacent to the base of the crista, with the "middle" and "shallow" electrodes progressively farther away, actual electrode array insertion depth can vary, and one canal's "deep" electrode could be farther from its target crista than another canal's "shallow" electrode is from its target. Because the magnitude and misalignment of prosthetically evoked VOR responses depend on actual electrode position and actual electrode-crista distance, while electrode array design engineers and surgeons can only control *intended* electrode position and *intended* electrode-crista distance, we aggregated and analyzed electrode performance both by actual distances measured using each animal's Solidworks model and by *intended* electrode position. To clarify this distinction, we capitalize "*Shallow*", "*Middle*" and "*Deep*" when referring categorically to an electrode's intended position (relative to others on the electrode array) and use the same terms without capitalization to refer to actual relative depths of insertion.

Results

Electrode Locations Measured via Computed Tomography

Computed tomography (CT) reconstructions (Fig. 3) confirmed that most horizontal and anterior stimulating

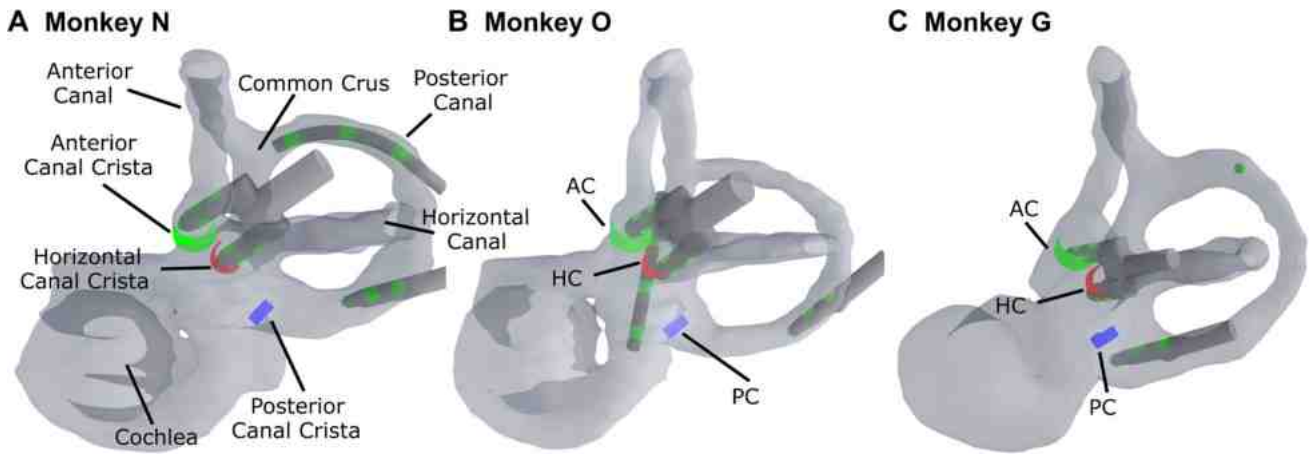

Fig. 3 Computed tomography reconstructions of the implanted inner ear of each animal included in this study. CT image data was segmented in 3D Slicer then imported into SolidWorks. The approximate position of the crista ampullaris in each canal is represented by a green (Anterior, AC), blue (Posterior, PC), or red (Horizontal, HC) crescent shape. The position of the crista was estimated by co-registering the animal's anatomy with a micro-MRI reconstruction of a normal monkey with no implant. Computer-aided design versions of electrode arrays were co-registered with the segmented electrodes. (**A**) Monkey N's horizontal canal electrode array was well positioned with the deepest electrode at the base of the crista while the anterior canal fork was slightly under-inserted. The posterior canal and *labyrinth return* arrays were also under-inserted. (**B**) Monkey O's horizontal and anterior canal arrays were slightly over-inserted but neither of the *Deep* electrodes was on the base of their respective crista. The posterior canal array was under-inserted, but the *labyrinth return* electrode array was over-inserted to the point where two of the electrodes ended up in the vestibule. The custom-fabricated return electrodes implanted in Monkey O's horizontal canal were not included in the CT reconstructions. (**C**) Monkey G's forked array was over-inserted in both canals further than that of Monkey O, but the posterior canal array was only slightly under-inserted. Monkey G's *labyrinth return* electrode (green sphere) was under-inserted with respect to the anterior/posterior canal junction of the CC

electrode arrays were in their target ampullae, while the posterior canal stimulating electrode arrays for Monkeys N and O were underinserted and in that canal's thin segment. For each stimulating electrode, Table 1 shows the measured distance to the base of the target canal's crista. Asterisks signify cases in which an electrode was deeper (along an insertion trajectory defined by the axis of that electrode's shank) than the base of the crista. Across all monkeys, electrode-target distances ranged from 0.18 to 4.61 mm. A rhesus ampulla lumen approximates an ellipsoid with length ~ 1.25 mm, breadth ~ 0.9 mm, and a crista projecting ~ 0.34 mm into the lumen from its anterior wall, so all electrodes within an ampulla should be within ~ 0.75 mm of that crista's base [18].

Table 1 Distance from each stimulating electrode to the base of its target crista. Measurements were made in SolidWorks as the shortest path within the bony labyrinth, which was always a straight line except for electrodes in a canal's thin segment (Fig. 3). Asterisks indicate cases in which an electrode was deeper (along a trajectory defined by the axis of that electrode's shank) than the base of its target crista. By that convention, most electrodes were underinserted. Monkey G's implanted electrode array did not include anterior or horizontal *Middle Inner* electrodes

Distance from Stimulating Electrode to Base of Crista Targeted (mm)					
Animal			Monkey N	Monkey O	Monkey G
Implanted Canal	Anterior	Shallow	1.28	1.11	0.53
		Middle Outer	0.85	0.61	0.2
		Middle Inner	0.43	0.39	-
		Deep	0.35	0.28*	0.52*
	Horizontal	Shallow	0.93	1.08	0.51
		Middle Outer	0.4	0.63	0.44*
		Middle Inner	0.33	0.26	-
		Deep	0.18*	0.23*	0.76*
	Posterior	Shallow	3.68	4.61	1.71
		Middle	2.94	3.86	1.12
		Deep	2.12	3.16	0.61

CT reconstructions also revealed positional variation for *labyrinth return* electrodes, which were inserted via a canalotomy in the posterior canal thin segment with the intent of landing them in the common crus. Monkey N's three *labyrinth return* electrodes were in the posterior canal thin segment 0.8–3.6 mm shallow to the common crus junction (CCJ) with the anterior and posterior canals. Monkey O's *labyrinth return* electrode array was 2.2–5.1 mm deeper than the CCJ. Monkey G's single return electrode ended up in the posterior canal 2.2 mm before the CC junction. For each animal, the return electrode closest to the CC junction was designated the "*common crus return*" electrode for performance comparisons between *common crus* and *distant return* electrodes.

Effects of Stimulating Electrode Position

Effects of Increasing Stimulus Current Amplitude on VOR Response Magnitude and Misalignment

VOR responses were elicited by prosthetic stimulation of each of the stimulating electrodes in all of the nine ampullae implanted for this study. As stimulus current amplitude was increased for a given stimulating/return electrode pair, phase duration and pulse rate, eye movement responses typically grew monotonically in speed (i.e., peak mean cycle-averaged magnitude of the 3D eye velocity vector during the slow-phase nystagmus driven by vestibular nerve activity during each 250 ms burst of 200 pulse/s stimulation, excluding saccadic quick phases). Responses aligned approximately with the anatomic axis of the targeted semicircular canal, which we use to define the ideal response direction.

Figure 4 shows cycle-averaged responses for stimulating/return electrode pairs in each of Monkey N's three implanted canals that elicited the largest VOR responses. Supplementary Figures S2 and S3 show the corresponding cycle-averaged VOR responses for the best performing stimulating/return electrode pairs in each canal of Monkeys O and G respectively. Stimuli delivered by the left anterior ampulla's best-performing electrode pair elicited up to a nearly 160°/s magnitude VOR response that grew linearly with stimulus currents above a ~ 100 µA/phase threshold (Fig. 4A) and aligned approximately with the ideal VOR response axis (i.e., the anatomic axis of the left anterior canal), as illustrated in Fig. 4 panels D-F. Stimuli delivered via the best electrode pair for the left posterior ampulla yielded eye movements predominantly aligned with the axis of the left posterior canal, which increased in magnitude with current amplitude. VOR magnitudes above ~ 230°/s were recorded for currents at and above 200 µA (Fig. 4B). Off-axis eye velocity components signifying current spread to the left anterior and horizontal canals were discernible at 75 µA, increased with stimulus current up to 175 µA, and plateaued at higher current amplitudes. Facial movement was observed at a current amplitude of 250 µA/phase (indicated by asterisks in Fig. 4), signifying facial nerve excitation due to current spread. The best electrode pair for the left horizontal ampulla yielded mainly horizontal eye movements (Fig. 4C). The presence of LARP and RALP components of eye velocity during stimulation is consistent with current spread causing spurious activation of afferent neurons that innervate the left anterior and posterior canals. A slight facial twitch was observed at 225 µA, and 250 µA reliably elicited facial movement.

As shown in Fig. 4E, F, the mean VOR response misalignment angle was 10°, 15° and 32°, respectively, for stimulation delivered at 250 µA using the anterior, posterior and horizontal canal's best-performing electrodes. Observed VOR axes for stimulation targeting the anterior canal are deviated toward the axis of the horizontal canal, and vice versa, consistent with the fact that the anterior and horizontal canal cristae and vestibular nerve branches are adjacent while the posterior canal's ampulla and nerve branch are relatively far away.

In summary, electrical stimulation delivered via electrodes implanted in each of the nine ampullae evoked VOR responses that generally increased with increasing current amplitudes. Comparable analyses revealed consistent results for Monkeys O and G (Figures S2 and S3). For the best performing stimulating electrodes, the VOR response magnitude ranged from 130 to 277°/s, while misalignment angles varied from 10 to 43° across all animals at the highest tested current amplitude. Notably, the observed VOR response axis and misalignment angle relative to the desired VOR axis depended heavily on the stimulating and return electrodes chosen and the current level tested, so the axes shown in Fig. 4F should not be mistaken for results that generalize for all combinations of electrodes and stimulus current.

Comparing Performance of Middle Inner versus Middle Outer Electrode Stimulation

Above we provided an overview of the magnitude and misalignment of VOR responses that were elicited by electrical stimulation; next we investigated the performance of stimulating electrodes by comparing *Middle Inner* versus *Middle Outer* electrodes. The performance of *Middle Inner* and *Middle Outer* electrodes was directly compared within each of four canals (i.e., the anterior and horizontal canals in Monkeys N and O) after quantifying VOR response magnitude and misalignment for each of the *Middle Inner* and *Middle Outer* stimulating electrodes when passing current in combination with each of the 6–9 possible return electrodes. The electrode array implanted in Monkey G did not include *Middle Inner* electrodes; therefore that animal was excluded from this analysis. Overall, *Middle Inner* and *Middle Outer* electrodes performed similarly. Figure 5 reveals that the *Middle Inner* electrodes in Monkey N's horizontal

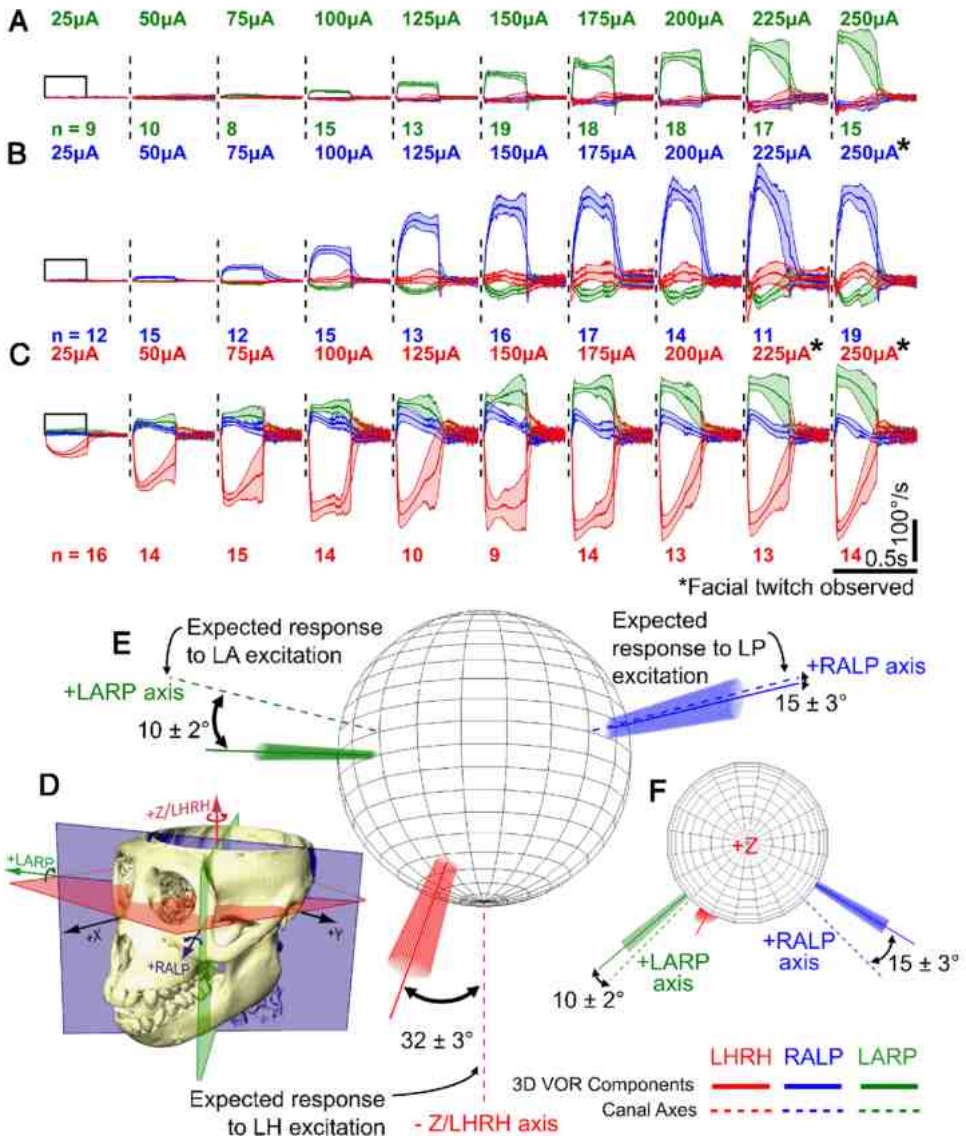

Fig. 4 Cycle averaged VOR responses to 200 μs/phase increasing stimulation current amplitude and response alignment with the target canal. For Monkey N, the mean ± standard deviation 3D VOR slow phase responses, averaged over n cycles, are shown when stimulating with 250 ms on, 250 ms off, 200 pulses/s, 200 μs/phase, biphasic, charge balanced pulse trains ranging from 25–250 μA in amplitude. The asterisk (*) denotes current amplitudes where a facial twitch was observed, and the black trace plotted during the first current step indicates at what point during the cycle stimulation was delivered. Stimulation was delivered by the *Shallow* electrode using the *Deep* as the return electrode (near-bipolar pair stimulation) (**A**) in the left anterior canal, (**B**) left posterior canal (facial twitch observed at 250 μA), and (**C**) in the left horizontal canal (a small fleeting facial twitch was observed at 225 μA but was sustained at 250 μA). The major horizontal component of slow phase VOR is negative in this case because stimulating the left horizontal canal drives the eye to the right, which, based on the right-hand rule, would be a negative rotation about the + Z/LHRH axis. (**D**) Canal and stereotaxic axis relative to landmarks on the animal's skull and a depiction of the direction of a positive rotation about a given axis based on the right-hand rule convention. (**E**) The peak 3D VOR slow phase in response to stimulation of each canal at 250 μA (during the first 100 ms of stimulation for each cycle) was extracted and then averaged by component over all accepted cycles and depicted as the mean axis of eye rotation by the solid lines. The conical plots around each mean rotation axis convey the variability of the axis of eye rotation over n accepted cycles and were calculated using the 3D VOR slow phase velocity covariance matrix and eigenvalue decomposition. Mean VOR misalignment ± standard deviation is the 3D angle between the axis of eye rotation and the anatomic canal axis depicted as dashed lines. (**F**) The data plotted in **E** are viewed along the + Z/LHRH axis from above the sphere

canal and Monkey O's anterior canal performed slightly better than the corresponding *Middle Outer* electrodes on average, yielding slightly larger VOR velocity magnitudes at the MAC; however, *Middle Inner* and *Middle Outer* electrodes performed similarly in Monkey N's anterior canal and Monkey O's horizontal canal.

Figure 6 further quantifies the comparison by showing the best observed performance (VOR magnitude and misalignment elicited by the MAC) for each middle electrode type, animal and canal, aggregating data over the 4 ampullae implanted with both *Middle Inner* and *Middle Outer* electrodes (Fig. 6A). *Middle Inner* electrodes elicited slightly larger VOR responses [$F_{[1, 38]} = 11.2$, and $p < 0.01$] (Fig. 6B) with no clear difference in misalignment [$F_{[1, 38]} = 2.7$, and $p > 0.05$] (Fig. 6C). For each shared return electrode, the VOR response elicited by a *Middle Outer* stimulating electrode was subtracted from that of a *Middle Inner* to create a single-value performance metric. Averaged over all possible combinations of animal, canal and return electrode (n = 30), the VOR magnitude (Fig. 6B) and misalignment (Fig. 6C) differences were 22 ± 7°/s (mean ± SEM) and 2 ± 1° respectively, consistent with a conclusion that *Middle Inner* electrodes outperformed *Middle Outer* electrodes on average, yielding larger VOR magnitudes with similar misalignments.

Comparing Performance of Shallow, Middle, and Deep Electrode Stimulation

After concluding *Middle Inner* stimulating electrodes elicit slightly larger eye movements than *Middle Outer;* we compared the performance of all stimulating electrodes within each implanted canal. The *Deep* stimulating electrodes consistently outperformed *Middle* and *Shallow* electrodes in 6 of the 9 canals tested (all of Monkey N's canals, in Monkey O's posterior and horizontal canals, and Monkey G's posterior canal). In the remaining 3 canals, no single stimulating electrode uniformly outperformed others, but the *Middle Inner* for Monkey O's anterior canal and the *Middle Outer* in Monkey G's anterior and horizontal canals elicited VOR magnitudes slightly higher than other electrodes in those canals. The next best stimulating electrode in each canal was always adjacent to the best electrode. For example, when the *Deep* electrode was the best, the *Shallow* electrode was never the next best. For each such animal/canal/stimulating/return electrode combination, Fig. 7A shows the VOR magnitude and misalignment measured at the MAC. Supplementary Figures S4–6 show VOR magnitude and misalignment for every animal, canal, stimulating electrode and return electrode.

Comparison of performance for the best and next best stimulating electrodes in each canal reveals that the 600–750 µm center-to-center spacing between adjacent electrodes within a canal corresponds to substantial differences in the efficacy of prosthetic stimulation. The best stimulating electrode yielded a larger VOR magnitude [$F_{[1,72]} = 56.1$, and $p < 0.001$] with no clear difference in misalignment [$F_{[1,76]} = 2.3$, and $p > 0.05$] compared to the next best stimulating electrode (Fig. 7). The VOR response elicited by the next best adjacent stimulating electrode in a given canal was subtracted from that of the best stimulating electrode in the same canal when the same return electrode was used. Averaged over all animals, canals and shared return electrodes tested, the mean VOR velocity and misalignment difference ± SEM was 61 ± 7°/s and -2.8 ± 1.5° respectively. Performing the same analysis but limited to cases when a *distant return* was used (which best represents the case of most VIs currently in use clinically [14, 16, 21, 35–39]), the best stimulating electrode yielded on average a 40 ± 12°/s larger VOR velocity [$F_{[1, 8]} = 6.5$, and $p < 0.05$] and a 5 ± 2.9° smaller (improved) misalignment [$F_{[1, 8]} = 3$, and $p > 0,05$] relative to the next best adjacent electrode. Similar results were found when confining the analysis to cases when a *CC return* was used. For those cases, the best stimulating electrode yielded a 54 ± 16°/s larger VOR velocity [$F_{[1, 8]} = 27$, and $p < 0.001$] and a 2 ± 3.7° smaller VOR misalignment [$F_{[1, 8]} = 0.5$, and $p > 0.05$] relative to the next best adjacent electrode.

Taken together, these results show that *the best-performing* stimulation electrodes significantly outperformed adjacent electrodes on average, yielding larger VOR magnitudes with similar misalignments. While this finding may not be surprising, these data are useful because they provide an estimate for the spatial precision with which a surgeon should implant a stimulation electrode. Viewing the *Deep*, *Middle* and *Shallow* electrodes' positions as different locations at which a surgeon might place a stimulating electrode for a VI that is limited to a single electrode per canal (e.g., to spare other stimulation channels for connection to a cochlear electrode array), these data show that a 600 µm change in surgical placement can have large and significant effects on device performance.

Effect of Stimulating Electrode Distance from Target Crista

We next investigated whether the distance from a stimulating electrode to its target canal's crista (Table 1) was a significant predictor of stimulation efficacy or selectivity and found it was correlated. For the best performing stimulating electrodes (one for each of the 9 canals), the mean distance to the target crista ± SEM was 0.9 ± 0.4 mm. Figure 8A shows VOR velocity and misalignment elicited at the MAC plotted against stimulating electrode position relative to the target canal crista when using a *distant return* electrode. Linear mixed effects models were implemented to quantify the relationship between stimulating electrode distance to target and VOR response by return electrode/animal/target canal. Generally, when using a *distant return* electrode, the VOR response appeared to improve (increased velocity) for stimulating electrodes closer to the target crista. The model showed that stimulating electrode distance to target was negatively correlated to VOR velocity [$\beta = -11$(°/s)/mm, SE = 10(°/s)/mm, $t = -1.1$] but not correlated to

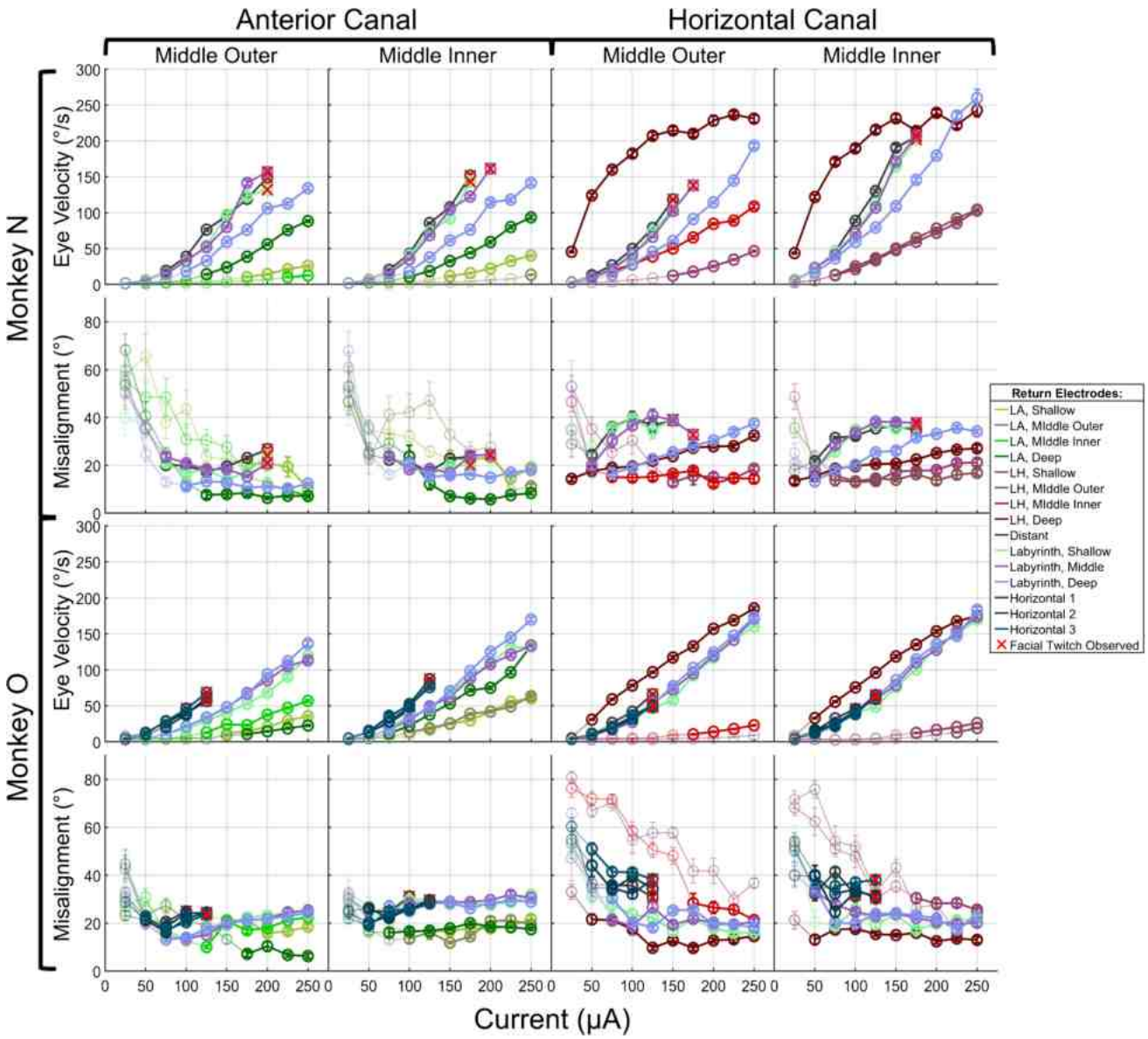

Fig. 5 Average slow phase VOR velocity and misalignment using *Middle Inner* and *Middle Outer* stimulating electrodes. Data for all possible return electrodes and tested current amplitudes are shown for Monkeys N and O (the only animals with *Middle Inner* and *Middle Outer* stimulating electrodes). Data are plotted as mean ± standard error of the mean over a minimum of n = 6 to a maximum of n = 20 cycles. Eye velocity magnitude was calculated using the maximum 3D VOR response during the first 100 ms of a given accepted cycle. The same 3D vector was used to calculate the 3D angle between the response axis and the stimulated canal axis. The magnitude and misalignment were then averaged over all accepted cycles. Stimulus current amplitude was systematically increased until 250 μA was reached or facial twitch was observed (marked with a red X), whichever came first. VOR magnitude and misalignment data points where the magnitude was less than 10°/s were faded. At the smaller current amplitudes, when the elicited VOR magnitude was small, misalignment values are large because this metric is susceptible to noise from the recording system with small eye movements

misalignment [β = 0.1°/mm, SE = 1.6°/mm, t = 0.074] when using a *distant return*. A similar analysis was conducted with VOR responses at the MAC when using a *CC return* electrode (Fig. 8B). The dependence of VOR magnitude and misalignment on electrode distance to crista was more pronounced when using a *CC* return rather than a *distant return*. The model revealed that stimulating electrode distance to target was significantly negatively correlated with VOR velocity [β = −49(°/s)/mm, SE = 10(°/s)/mm, t = −4.7] and positively correlated with misalignment [β = 4.8°/mm, SE = 1.7°/mm, t = 2.9]. These findings are consistent with the conclusion that increasing stimulating electrode distance to the target canal's crista decreases stimulation efficacy and selectivity, yielding smaller eye movements with larger misalignment.

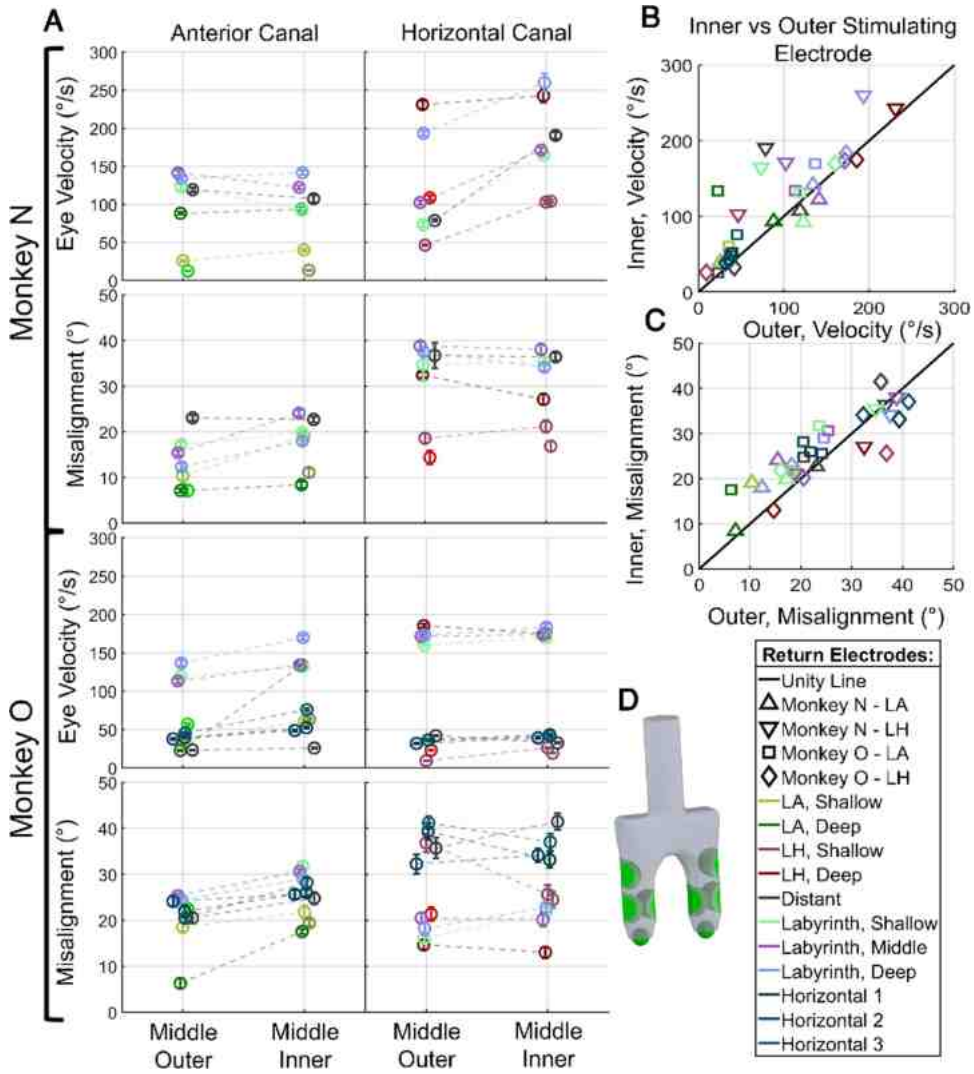

Fig. 6 VOR responses at the maximum allowable current amplitude—*Middle Inner* vs. *Middle Outer* stimulating electrode. (**A**) For each combination of stimulating and return electrode in Fig. 5, the VOR mean ± standard error of the mean (**SEM**) magnitude and misalignment at the highest current amplitude tested before observing facial twitch was extracted. Dashed lines show data points to be compared since the same return electrode was used. This allows for direct comparison of the practical performance between *Middle Inner* and *Middle Outer* electrodes. (**B**) From the data plotted in panel A, for each animal, the VOR magnitude response elicited when using a *Middle Inner* electrode was plotted against that of a *Middle Outer* electrode when the same return electrode was used. Data points corresponding to Monkey N are triangles with the upward pointing triangle corresponding to electrode combinations from the anterior canal while downward pointing triangles represent electrode combinations from the horizontal canal. Data points corresponding to Monkey O are either squares (stimulating the anterior canal) or diamonds (stimulating the horizontal canal). The solid black line is a unity line to be used as a visual reference. Most data points are above the unity line, indicating the VOR magnitude elicited by a *Middle Inner* electrode was greater than that of a *Middle Outer* electrode when the same return electrode was used. (**C**) VOR misalignment responses at the MAC are visualized in the same manner as VOR magnitude responses in panel B. The data points are more tightly centered around the unity line but still sit slightly above the line, indicating a *Middle Inner* electrode elicits slightly larger misalignment than that of a *Middle Outer* electrode. (**D**) Computer-aided design of the forked electrode array to provide a visual representation of *Middle Inner* and *Middle Outer* electrode position on the array

Effect of Return Electrode Position

Analyses analogous to those above were further performed to compare performance using different return electrodes for a given stimulating electrode. For each stimulating electrode, we measured and compared performance using a *distant return* electrode (in neck muscle outside the temporal bone), *common crus return* electrode (i.e., a *labyrinth return* electrode in or near the common crus) and *ampullary return* electrodes (i.e., using the other electrodes on the same shank as a stimulating electrode under study as a return electrode).

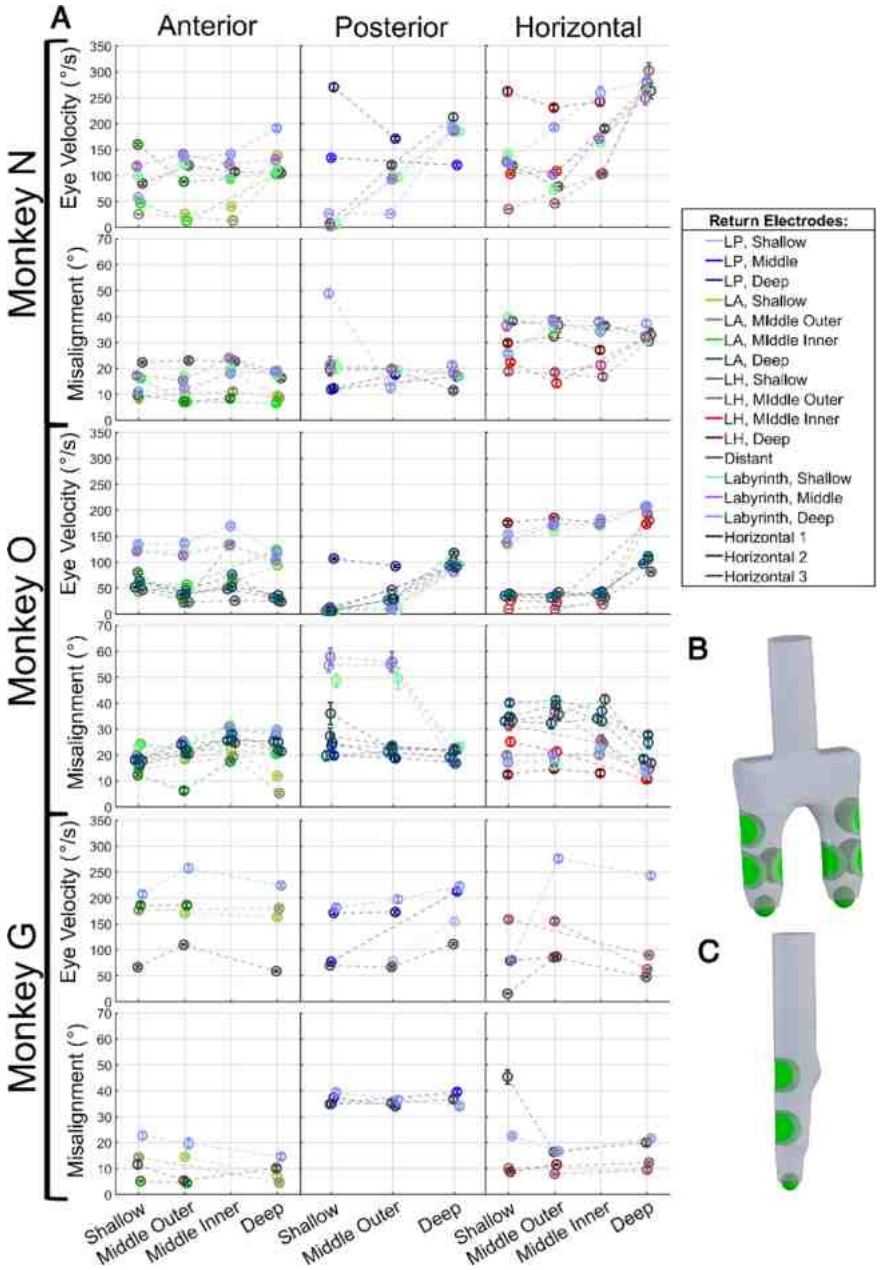

Fig. 7 VOR responses at the maximum allowable current amplitude using a *Shallow, Middle Inner, Middle Outer,* and *Deep* stimulating electrode. (**A**) For each stimulating and return electrode combination tested for all three animals, the VOR mean ± SEM magnitude and misalignment response at the MAC are presented. Dashed lines show instances where, within a given canal, for each of the connected stimulating electrode data points, the same return electrode was used (also conveyed by color). Data points are not present for Monkey G in the *Middle Inner* stimulating electrode column because that animal did not have those electrodes on the implanted array. For each stimulating electrode, the VOR magnitude responses were aggregated over all return electrodes tested. The mean VOR magnitude could then be compared within each canal to yield a rough estimate for the best and the next best performing stimulating electrodes. For Monkey N, the best and next best performing stimulating electrodes elicited a mean ± SEM VOR magnitude over all tested return electrodes (n = 6 or 7) of 127 ± 12°/s (*Deep*) and 92 ± 20°/s (*Middle Outer*) in the anterior canal, 181 ± 13°/s (*Deep*) and 101 ± 19°/s (*Middle Outer*) in the posterior canal, and 272 ± 7°/s (*Deep*) and 177 ± 23°/s (*Middle Inner*) in the horizontal canal. For Monkey O, the best and next best performing stimulating electrodes elicited a mean ± SEM VOR magnitude over all tested return electrodes (n = 9 or 10) of 90 ± 15°/s (*Middle Inner*) and 79 ± 11°/s (*Shallow*) in the anterior canal, 96 ± 3°/s (*Deep*) and 29 ± 9°/s (*Middle Outer*) in the posterior canal, and 157 ± 16°/s (*Deep*) and 90 ± 23°/s (*Middle Inner*) in the horizontal canal. For Monkey G, the best and next best performing stimulating electrodes elicited a mean ± SEM VOR magnitude over all tested return electrodes (n = 4) of 181 ± 30°/s (*Middle Outer*) and 159 ± 31°/s (*Shallow*) in the anterior canal, 176 ± 26°/s (*Deep*) and 129 ± 33°/s (*Middle Outer*) in the posterior canal, and 151 ± 45°/s (Middle Outer) and 111 ± 45°/s (*Deep*) in the horizontal canal. For reference, we show a computer-aided design depiction of the forked electrode array implanted in the horizontal and anterior canals (**B**) and the linear electrode array implanted in the posterior canal (**C**)

Comparing Performance of Common Crus versus Distant Return Electrodes

To better understand the role of return electrode location on vestibular implant stimulation efficacy, we compared VOR responses elicited when using a *CC* and *distant return*. As shown by CT scan reconstructions (Fig. 3), insertion of return electrodes into the posterior canal with the intent of targeting the midpoint of the common crus resulted in insertion depths that varied widely between different animals, with electrodes either under- or over-inserted relative to the midpoint of the common crus junction (the junction of the anterior and posterior canals). For comparisons between different return electrode locations, we classified the return electrode closest to the common crus in each animal as the *CC return* and then compared performance for all stimulating electrodes using either a *CC return* or a *distant return* electrode. For Monkey N, the *CC return* was the deepest *labyrinth return* electrode. For Monkey O the shallowest *labyrinth return* was used. Monkey G only had a single *labyrinth return* electrode and that was defined as the *CC return* for that animal.

Overall, we found that *CC return* electrodes outperformed corresponding *distant return* electrodes, yielding significantly larger VOR responses [$F_{[1, 30]} = 32$, and $p < 0.001$] and similar misalignment [$F_{[1, 30]} = 0.03$, and $p > 0.05$] at the highest stimulus current that did not elicit facial twitch. An initial comparison of using either a *CC* or *distant return* (Fig. S7) shows that Monkey N's *distant return* elicited a facial twitch with 9 of the 11 stimulating electrodes at an average current amplitude of 181 μA, while the *CC return* yielded facial movement with 2 of 11 stimulating electrodes at 200 and 250μA. Monkey O's *distant return* yielded facial movement with 9 of 11 stimulating electrodes at an average current amplitude of 119 μA, while facial twitch was only observed with 2 of 11 stimulating electrodes using the *CC return* at 125 and 150 μA. Using a *distant return* with Monkey G resulted in facial movement for all 9 stimulating electrodes at 100 μA, while using a *CC return* for Monkey G yielded facial movement in 6 of 9 stimulating electrodes, all at 250 μA. For all three animals, when comparing VOR responses at the MAC (Fig. 9A), the *CC return* appeared to be the best-performing return electrode, yielding an average VOR magnitude ± SEM (for all stimulating electrodes tested) of 148 ± 26°/s. 114 ± 19°/s and 210 ± 19°/s for Monkeys N, O and G, respectively, compared to 128 ± 21°/s, 43 ± 8°/s, and 70 ± 10°/s when using a *distant return*.

To further quantify these observations, VOR magnitude (Fig. 9B) and misalignment (Fig. 9C) elicited by a *distant return* at the MAC were subtracted from corresponding values measured using a *CC return*, aggregating paired data over all stimulating electrodes. Averaged over all 31 possible combinations of animal, canal and stimulating electrode, *CC return* electrodes outperformed *distant return* electrodes by an average VOR magnitude of 73 ± 13°/s, while VOR misalignment was similar for the two return electrode types, with a mean difference of 1 ± 2.2°, consistent with a conclusion that *CC return* electrodes outperformed *distant return* electrodes on average, yielding larger VOR magnitudes with similar misalignments.

Comparing Performance of Common Crus vs. Labyrinth and Vestibule Return Electrodes Across Monkeys

After concluding that a *CC return* outperforms a *distant return* electrode, we compared the performance of return electrodes in and around the CC to better understand the effect of return electrode position within the labyrinth (but outside the ampullae) on elicited VOR responses. Monkey G was excluded from this analysis because that animal was only implanted with a single return electrode within the labyrinth that was outside of the ampullae. The analysis was performed separately for Monkeys N and O because the return electrode array intended to be implanted in the CC was either mostly over-inserted (residing mostly in the vestibule) or under-inserted (residing mostly in the posterior canal). Overall, *CC return* electrodes performed similarly to those in either the posterior canal or the vestibule.

Common Crus versus Labyrinth Return Electrodes

Monkey N's *labyrinth return* electrode array was mostly in the thin segment of the posterior semicircular canal, with only its deepest return electrode near the common crus (and therefore defined as that animal's *CC return*). All three *labyrinth return* electrodes performed similarly in that animal. The *CC return* yielded no difference in VOR magnitude [$F_{[2, 20]} = 3$, and $p > 0.05$] or misalignment [$F_{[2, 20]} = 0.5$, and $p > 0.05$] relative to either of the other two return electrodes. When using the *CC return*, facial twitch was observed with 2 of 11 stimulating electrodes at 200 and 250 μA as opposed to 8 of 11 at an average of 190.6 μA for the *Middle labyrinth return* and 9 of 11 at an average of 186.1 μA for the S*hallow labyrinth return* (Fig. S8). Comparing VOR responses at the MAC (Fig. 10A), the *CC return* appeared to be the best-performing return electrode yielding an average VOR magnitude ± SEM (for all stimulating electrodes) of 148 ± 26°/s, the *Middle* was the next best (131 ± 19°/s) and was similar to the *Shallow* (123 ± 20°/s).

To further quantify these observations, VOR magnitude (Fig. 10B) and misalignment (Fig. 10C) elicited when using Monkey N's *Middle* or *Shallow labyrinth returns* at the MAC were subtracted from that of the corresponding *CC return* using the same stimulating electrode. Averaged over all 22 possible combinations of canal and stimulating electrode, the mean VOR magnitude and misalignment

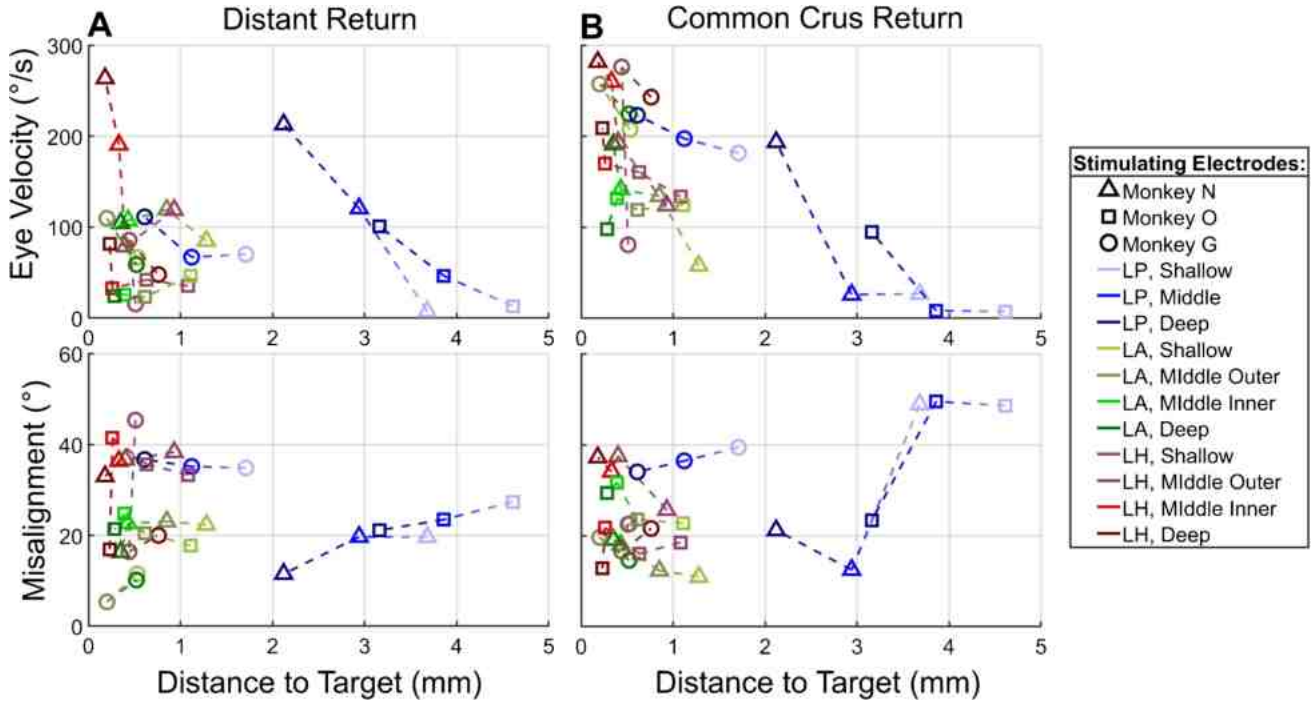

Fig. 8 Dependence of VOR response on stimulating electrode distance to target canal crista, grouped by return electrode. Each animal's data is represented by a different shape, and each color represents a different stimulating electrode. Dashed lines link data points from the same canal by animal. (**A**) VOR magnitude and misalignment elicited using a *distant return* at each stimulating electrode's maximum allowed current (MAC). (**B**) VOR magnitude and misalignment elicited using a *common crus return* at MAC

differences were $21 \pm 12°$/s and $0.3 \pm 2.2°$ respectively, consistent with a conclusion that the performance of the *CC return* electrode was comparable to that of the other *labyrinth return* electrodes on average, yielding slightly larger VOR magnitudes with similar misalignments. Analysis of Monkey O's data (Fig. S9 and S10) yielded similar results.

Comparing Performance of Ampullary, Common Crus and Distant Return Electrodes

To better understand the effect of return electrode proximity to a targeted vestibular nerve branch and a given stimulating electrode, we compared the eye movements elicited by *ampullary*, *CC*, and *distant return* electrodes. The best-performing *ampullary return* electrode for each canal typically outperformed *CC return* and *distant return* electrodes, yielding large improvements in VOR magnitude [$F_{[1, 21]} = 46$, and $p < 0.001$] and misalignment [$F_{[1, 21]} = 51$, and $p < 0.001$] relative to results achieved using a *distant return* and large improvement in VOR misalignment [$F_{[1, 21]} = 39$, and $p < 0.001$] without much change in magnitude [$F_{[1, 21]} = 1$, and $p > 0.05$] relative to a *CC return*. For all 9 canals studied except Monkey G's horizontal canal, the best-performing *ampullary return* electrode was the *Deep* electrode contact (Fig. 11A). For Monkey G's horizontal canal, the best-performing *ampullary return* electrode was the *Middle* electrode. For Monkeys N and O, the facial twitch threshold was similar when using the best *ampullary return* electrode as compared to the *CC return*, which was much higher than when using a *distant return*. For Monkey G, facial twitch was not observed when using the best *ampullary returns* but was observed with most stimulating electrodes when using a *CC return* and all stimulating electrodes when using a *distant return* (Fig. S11-13).

VOR magnitude (Fig. 11B) and misalignment (Fig. 11C) elicited by stimulation at the MAC when using the best *ampullary return* in each canal was compared to using a *distant return* for each of the 22 stimulating electrodes, and results were averaged over those 22 data pairs. *Ampullary return* electrodes outperformed *distant returns*, with a mean VOR magnitude difference of $90 \pm 14°$/s and a misalignment difference of $-11 \pm 2°$. The same analysis was applied to a comparison of VOR magnitude (Fig. 11D) and misalignment (Fig. 11E) elicited by an *ampullary* versus *CC return*. The mean velocity difference was $21 \pm 19°$/s and the mean misalignment difference was $-11 \pm 2°$. These results are consistent with a conclusion that the best-performing *ampullary return* electrode outperforms *distant* and *CC return* electrodes on average, yielding larger VOR magnitudes as compared to those elicited by a *distant return* with smaller (improved) misalignments.

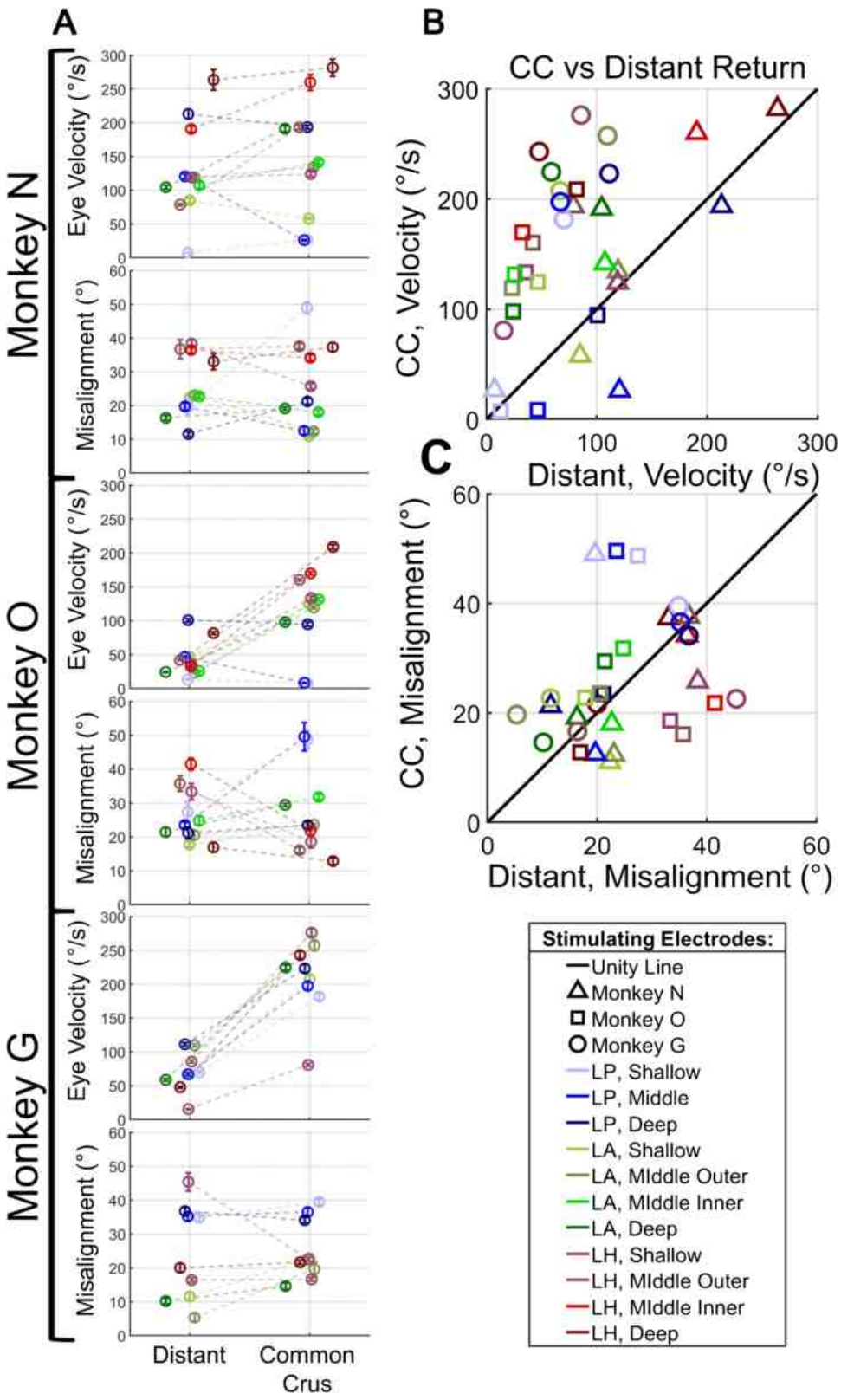

Fig. 9 VOR responses at the maximum allowable current amplitude (MAC) using either a *Distant* or *Common Crus return*. (**A**) For each stimulating electrode when using either a *distant* or *CC return*, VOR mean ± SEM magnitude and misalignment response at the MAC are presented. Dashed lines connect data points showing the response when using the same stimulating electrode with either a *distant* or *CC return* (also conveyed by color), facilitating comparison of performance between *distant* and *CC return* electrodes. (**B**) VOR magnitude elicited using a *CC return* plotted against responses using a *distant return* with the same stimulating electrode. Triangle, square and circle markers show data for Monkeys N, O and G, respectively. Most data points lie well above the unity line (black), indicating better performance with a *CC return* electrode. (**C**) VOR misalignment responses at the MAC compared as in panel B scatter equally around the unity line, indicating lack of a significant difference in VOR misalignment elicited by a *CC* or *distant return* electrode

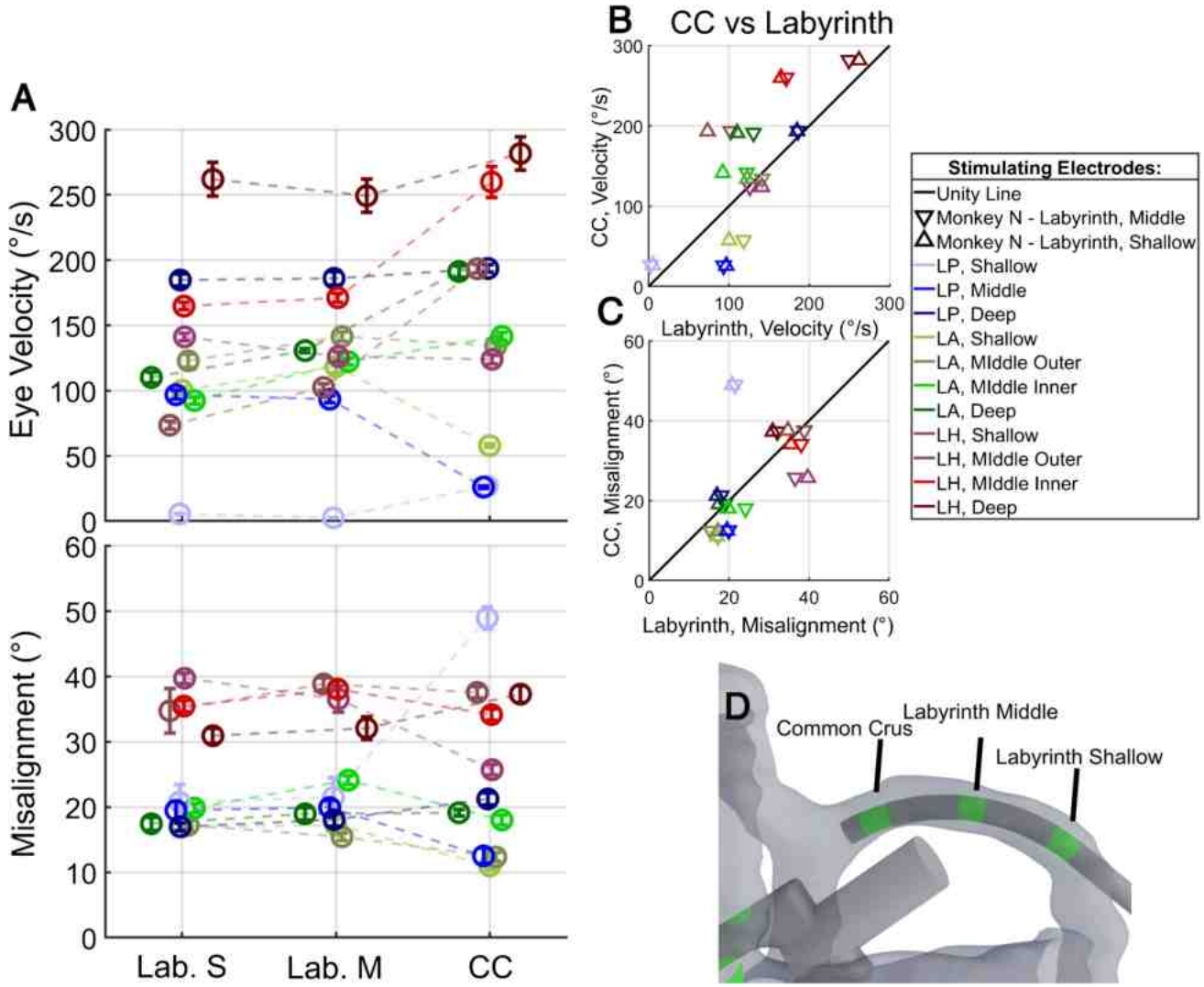

Fig. 10 VOR response at the maximum allowable current (MAC) for Monkey N when using a *Common Crus* or *Labyrinth return*. (**A**) For each stimulating electrode when using either a *labyrinth Shallow (Lab. S), labyrinth Middle (Lab. M),* or *CC return* in Monkey N, the VOR mean ± SEM magnitude and misalignment response at the MAC are presented. Dashed lines connect data points showing the elicited response when using the same stimulating electrode with either a *labyrinth Shallow, labyrinth Middle,* or *CC return* (also conveyed by color). (**B**) VOR magnitude using a *CC return* plotted against that of either a *labyrinth Middle* or l*abyrinth Shallow return* when the same stimulating electrode was used. Triangles pointing down compare responses elicited by a *CC return* versus *labyrinth Middle return*; triangles pointing up compare *CC return* versus *labyrinth Shallow return*. Data are scattered above and below the unity line (black). (**C**) VOR misalignment data at MAC compared as in panel B. (**D**) View of Monkey N's electrodes

Discussion

The focus of this study was to explore relationships between prosthetically evoked VOR responses and positions of a VI's stimulating and return electrodes. Our exploration was motivated by two goals. First, we sought to identify where a surgeon should position stimulating and return electrodes to simultaneously maximize both the efficacy and selectivity of prosthetic stimulation targeting individual branches of the vestibular nerve. Second, we reasoned that if a single optimal position could be identified for each semicircular canal ampulla, then one could design a VI that only needs a total of 3 stimulation channels to effectively stimulate the implanted ear's 3 semicircular canals, rather than using multiple stimulating electrodes per canal in hope that at least one will work well. Reducing the number of electrodes required per ampulla would be beneficial because the total number of stimulation channels is limited for VIs, as it is for the CIs from which they are adapted. For example, the implant used in the only published clinical study of long-term continuous use of VIs for treatment of bilateral vestibular hypofunction was limited to 12 channels, with 9

devoted to vestibular stimulation [14, 16]. (Each of the 3 semicircular canals was implanted with an array containing 3 electrodes, and the device's remaining 3 stimulation channels went unused.) If each of the three canals only requires a single, optimally positioned electrode to achieve effective and selective vestibular nerve branch stimulation, then the remaining 9 electrodes could be used to make an effective CI array. The resulting vestibular-cochlear implant system could be used to treat patients with combined canal and cochlear dysfunction, or its cochlear array could be banked in the body at the time of vestibular implantation, held in reserve for implantation into the cochlea during a second surgery if the patient develops hearing loss. Alternatively, the stimulation electrode channels freed up by optimizing ampullary stimulation electrode position based on the current study's results could instead be adapted to target the utricle and/or saccule.

We started with a comparison of *Middle Inner* and *Middle Outer* electrodes to determine whether their performance differs enough to merit considering an electrode design change for electrode arrays currently used in the clinical trial at our institution (which currently have Middle Outer electrodes but no Middle Inner electrodes). The motivation for testing the performance of a *Middle Inner* or *Middle Outer* electrode contact on the anterior and horizontal canal shanks stems from the path taken by the nerve branches that originate in those canals. Vestibular nerve branches that innervate the anterior and horizontal canal cristae only separate as they emerge from the internal auditory canal near the junction of those two ampullae [42]. Therefore, electrodes on the outer surface of the shank are farther away from the cristae and nerve branches than electrodes on the inside of the shank. In the present study, stimulating via an *Inner* electrode contact yielded a slight improvement in VOR magnitude with no difference in VOR misalignment as compared to an *Outer* electrode. This finding, in a limited data set of 4 implanted canals, suggests that future designs of the forked array should include either a *Middle Inner* or *Outer* electrode but not both. While many combinations of stimulating and return electrode pairs were tested, this comparison was only conducted in two animals. That, along with variability in placing the electrode array during surgery, could limit the generalizability of the findings.

While a *Middle Inner* slightly outperformed a *Middle Outer* stimulating electrode in these animals, our study's second aim was to determine the best design and placement of stimulating electrodes on a given shank. Overall, we found that deeper stimulating electrodes performed best in most canals tested. In specific cases where the deepest was not the best performing stimulating electrode, the electrode array had been over-inserted so that the *deepest* stimulating electrode was pushed past the target canal's crista (Fig. 3B, C). These results align with intuition and with quantitative model predictions by Hedjoudje et al. 2019 that the electrode closest to the targeted canal's crista should most effectively recruit afferents from that branch of the vestibular nerve [18].

Because the best stimulating electrode always yielded more effective stimulation than the next best adjacent electrode, we know that the 600 µm center-to-center inter-electrode distance substantially changes stimulating electrode performance, and we can infer that electrode array designs and surgical techniques should therefore reflect the need to place stimulating electrodes within 600 µm of their target to avoid suboptimal performance.

Intraoperative image guidance and electrophysiological measurement have been proposed as aids to achieving optimal electrode placement [43, 44]. An augmented reality display of inner ear structures aligned to invariant temporal bone features might provide a visual representation of the electrode array position relative to the target [45–49]. Intraoperative electrophysiological measurements might help identify the optimal position of an electrode relative to target neurons. For example, vestibular electrically-evoked compound action potentials (veCAPs) have been used to measure neuronal recruitment in response to electrical stimulation from a given electrode [41, 42, 44, 50–58].

A third aim of our study was to compare return electrode performance. The VI system we currently study in a clinical trial has a single return electrode, which has either been placed distally or within the labyrinth [14, 16, 21, 35–39]. In the present animal study, we found that *CC return* electrodes typically yield better overall performance than *distant return* electrodes. Using a *distant return* resulted in a lower current threshold for eliciting eye movements (due in part to the stimulation at the target being monopolar) than a *CC return* electrode; this also resulted in a lower threshold for eliciting a facial twitch. That has also been observed in data published for human VI recipients [14, 15]. Moreover, the MAC was often limited by facial twitch when using a *distant return*, whereas stimulation using a *CC return* was more selective and yielded larger eye movements without facial twitch. These empirical data are consistent with computational modeling, which predicted that a *CC return* electrode should yield more targeted stimulation than a *distant return* [18].

Return electrode arrays we intended to implant in the common crus of Monkeys N and O ended up in very different positions, with the former barely reaching the common crus while the latter mostly passed through the common crus and ended up in the vestibule. Within-animal comparisons showed no difference in performance between the three return electrodes in Monkey N and only a slight difference in elicited VOR magnitude between the three return electrodes in Monkey O. These data suggest there is only a slight if any difference in stimulation efficacy across a 3 mm span for return electrodes near the common crus extending either

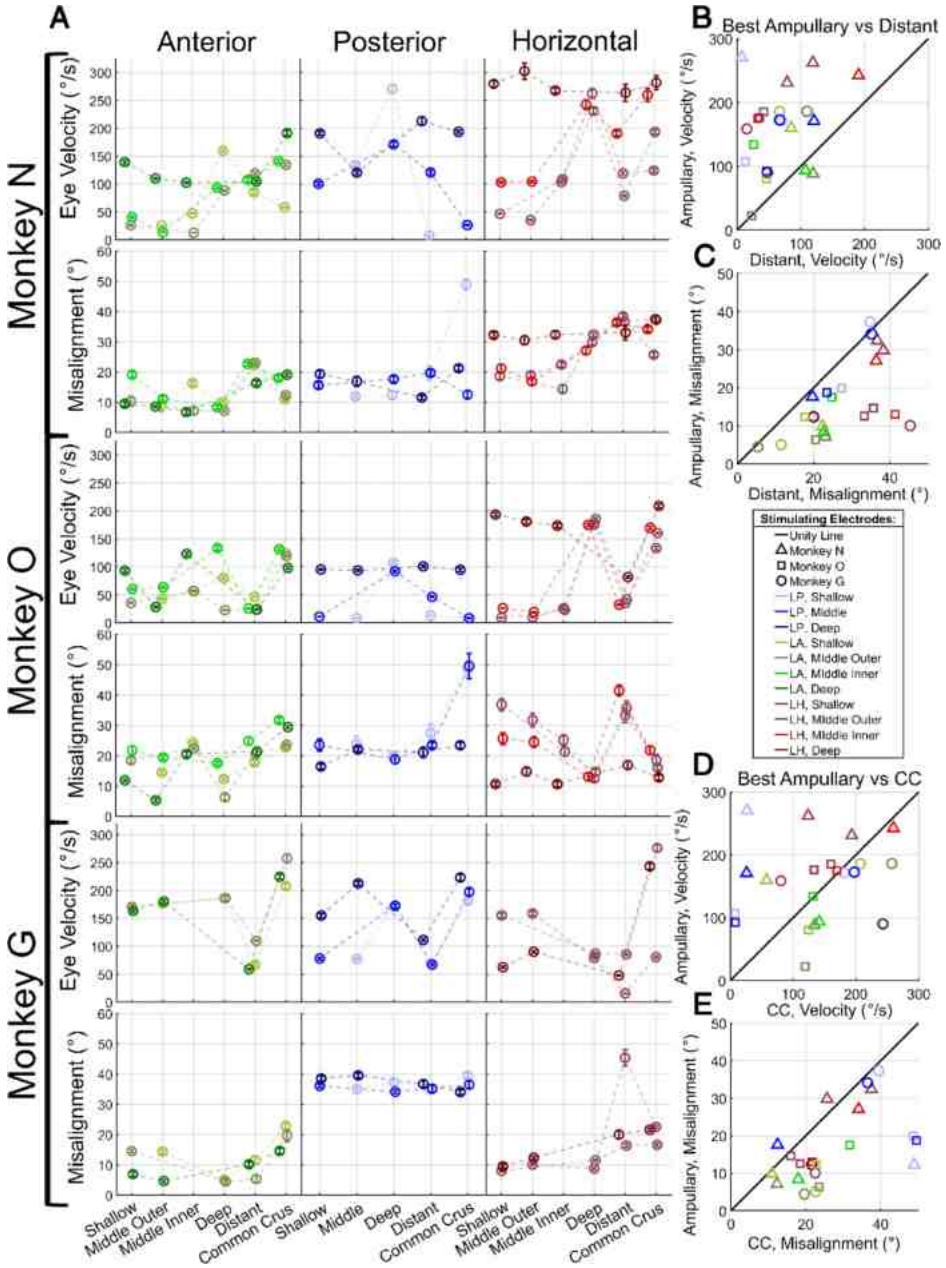

Fig. 11 VOR responses at the maximum allowable current (MAC) when using an *Ampullary, Distant, and CC* return electrode. (**A**) For each stimulating and return electrode combination tested for all three animals, VOR mean ± SEM magnitude and misalignment at MAC are presented. Dashed lines connect data points showing the elicited response when using the same stimulating electrode with either an *ampullary, distant,* or *CC return*. Monkey G did not have a *Middle Inner* electrode. For each return electrode, VOR magnitudes were aggregated over all stimulating electrodes tested. Mean VOR magnitude was compared within each canal to identify the best performing *ampullary return* electrodes. For Monkey N, the best performing *ampullary return* electrodes elicited a mean ± SEM VOR magnitude over all tested stimulating electrodes ($n=2$ or 3) of 114 ± 23°/s (*Deep*) in the anterior canal, 221 ± 50°/s (*Deep*) in the posterior canal, and 245 ± 9°/s (*Deep*) in the horizontal canal. For Monkey O, the best performing *ampullary return* electrodes elicited a mean ± SEM VOR magnitude over all tested stimulating electrodes ($n=2$ or 3) of 79 ± 32°/s (*Deep*) in the anterior canal, 100 ± 7°/s (*Deep*) in the posterior canal, and 179 ± 3°/s (*Deep*) in the horizontal canal. For Monkey G, the best performing *ampullary return* electrodes elicited VOR magnitudes over all tested stimulating electrodes ($n=2$) of 186 and 186°/s (*Deep*) in the anterior canal, 172 and 173°/s (*Deep*) in the posterior canal, and 159 and 90°/s (Middle Outer) in the horizontal canal. (**B**) From the data plotted in panel **A**, for each animal, the VOR magnitude response elicited when using the best *ampullary return* in each canal was plotted against that of a *distant return* when the same stimulating electrode was used. Triangles, squares and circles show data from Monkeys N, O and G, respectively. Almost all data points lie well above the unity line (black), so by VOR magnitude the best *ampullary return* electrode outperformed the *distant return* electrode when used at each stimulating electrode's MAC. (**C**) Plotting VOR misalignment at MAC for the best *ampullary* versus *distant return* electrode reveals that the best *ampullary return* outperformed the *distant return*. Comparison of the best *ampullary return* and *CC return* reveals no consistently best performer by magnitude (**D**), but better performance by *ampullary return* electrodes for VOR alignment (**E**) [40, 41]

into the posterior canal or the vestibule (i.e., the center-to-center distance from the *Deep return* to the *Shallow return* electrode). These data conflict with computational modeling that predicted placing a return electrode deeper within the CC would yield more targeted recruitment over that placed shallower within the CC [18].

Clinical VI trials have focused mainly on monopolar stimulation and far-bipolar stimulation (with the return electrode in the common crus or in a different ampulla), while near-bipolar stimulation between two electrodes within the same canal remains relatively understudied in humans [14, 16, 21]. However, using an *ampullary return* should theoretically yield more focused stimulation allowing for improved targeting over a *CC* or *distant return*. Indeed, here we found that using the best *ampullary return* was more selective than using a *distant* or *CC return* and was more effective than using a *distant return*. There were instances when a *CC return* yielded much larger eye movements than an *ampullary return* when the same stimulating electrode was used and there were cases when the opposite was true. However, the *ampullary return* yielded eye movements that were better aligned with the target canal axis. The fact that the best *ampullary returns* outperformed the *distant return* suggests that future designs of VIs should include a *CC return* and the ability to deliver near-bipolar stimulation using an *ampullary return*.

Since the ability to deliver electrical stimulation using near-bipolar electrode pairs clinically would, in some cases, require a modification of stimulator hardware, this topic warrants further investigation. Specifically, the effect of inter-electrode distance when using near-bipolar stimulation should be explored. There could be an optimal distance between the stimulating and ampullary return electrode that yields the largest eye movements with the smallest degree of misalignment. Additionally, the effect of using a continuous and large stimulating electrode starting at the tip and traversing some distance up each shank should be tested both computationally and empirically. While placing a single electrode at the tip of each shank may theoretically be sufficient, that design would not accommodate the variability in placing stimulating electrodes observed in this work. However, assuming the larger electrode design elicits similar VOR responses to those elicited by electrodes used currently, the single large electrode design would act as a hedge against placement variability while freeing up the necessary channels for a CI.

Limitations of this study include differences between anatomy and preimplant status between the monkeys we studied and human VI candidates. Labyrinth anatomy is similar across all primates, but the rhesus labyrinth is smaller (e.g., canal thin segment caliber is ~ 1 mm in humans and ~ 0.6 mm in rhesus), so our electrode arrays were about 60% of the size we used in humans. Compared to our VI implantation technique for humans, the anterior-horizontal canal electrode array insertion trajectory was constrained somewhat by the paraflocculus, which in monkeys mostly fills the volume subtended by the three semicircular canals [18, 20]. To avoid dura near the paraflocculus, we made ampullotomies slightly more lateral in monkeys and therefore insert along trajectories that are a little more medially directed than the trajectory used for humans. In contrast to human VI candidates, Monkeys N and O had normal labyrinths before implantation, because they were also subjects in a parallel study of single-unit electrophysiologic recording, for which preservation of some mechanosensitivity helps identify the source end organ for isolated vestibular nerve primary afferent neurons. However, VI-driven VOR responses for those monkeys (Fig. 7) were similar to those for Monkey G, which had bilateral vestibular hypofunction caused by intratympanic gentamicin injection (for a study characterizing VOR responses to head rotation before and after ototoxic injury) for 8 years before these experiments started.

Despite those limitations, the present study has shown that (1) stimulating electrode position is a key factor in stimulation efficacy; (2) although using a *distant return* results in lower stimulation thresholds, *labyrinth* and *ampullary returns* are more effective because they yield more spatially selective stimulation; and (3) near-bipolar stimulation between electrodes within a target ampulla should outperform other approaches as long as electrodes can be positioned with sufficient accuracy and can deliver sufficiently high currents.

Supplementary Information The online version contains supplementary material available at https://doi.org/10.1007/s10162-025-01020-0.

Acknowledgements The authors thank Kelly Lane for her help with the care of animals included in this study, MED-EL GmbH for fabricating the electrodes, Gene Fridman PhD for feedback and comments on this manuscript, and Wojtek Zbijewski, Ali Uneri, and Yixuan Huang and members of the JHMI Carnegie Center for Surgical Innovation for help acquiring computed tomography image data used for this study. We would also like to acknowledge Peter Boutros PhD and Chenkai Dai MD PhD for their help with building up and passing along the knowledge of conducting research with non-human primates in the Vestibular NeuroEngineering Lab.

Author Contribution B.J.M. and C.C.D.S. designed the experiments included in this study. D.C.R. designed and constructed the experimental setup. R.H. manufactured electrode arrays. B.J.M. conducted the experiments. B.J.M., K.N.M., and C.C.D.S. analyzed the data. B.J.M., K.N.M., C.F.B., K.E.C., and C.C.D.S. interpreted the results. B.J.M., K.N.M., and C.F.B. created the figures. B.J.M. drafted the manuscript. B.J.M., K.N.M., C.F.B., K.E.C., and C.C.D.S. provided feedback on and edited the manuscript. B.J.M., K.N.M., C.F.B., D.C.R., R.H., K.E.C., and C.C.D.S. approved the final manuscript.

Funding This research was supported by National Institute on Deafness and Other Communication Disorders grants R01DC009255, R01DC013536, R01DC002390, F31DC019861, and T32DC000023; MED-EL GmbH; and contributors to the Johns Hopkins Vestibular NeuroEngineering Lab Research Fund.

AI was not used for research purposes nor for manuscript preparation.

Data Availability All scripts used for analysis and data included in this study are publicly available through the Johns Hopkins University Research Data Repository.

Declarations

Ethics Approval Three adult female rhesus monkeys (*Macaca mulatta*, Monkeys N [RhF73AN], O [RhF80CO], and G [RhF60738G]) were studied in these experiments, which were conducted under a protocol approved by the Johns Hopkins Animal Care and Use Committee, accredited by the Association for the Assessment and Accreditation of Laboratory Animal Care (AAALAC) International.

Conflict of interest C. C. Della Santina holds an equity interest in Labyrinth Devices, LLC, which is working to develop a vestibular implant for clinical use through a collaboration with Johns Hopkins School of Medicine and MED-EL GmbH. The terms of that arrangement are managed in accordance with Johns Hopkins University policies on conflicts of interest and interaction with industry.

References

1. Ward BK, Agrawal Y, Hoffman HJ, Carey JP, Della Santina CC (2013) Prevalence and impact of bilateral vestibular hypofunction: results from the 2008 US National Health Interview Survey. JAMA Otolaryngol Head Neck Surg 139:803–810
2. Sun DQ, Ward BK, Semenov YR, Carey JP, Della Santina CC (2014) Bilateral vestibular deficiency: quality of life and economic implications. JAMA Otolaryngol Head Neck Surg. https://doi.org/10.1001/jamaoto.2014.490
3. Black FO, Gianna-Poulin C, Pesznecker SC (2001) Recovery from vestibular ototoxicity. Otol Neurotol 22:662–671
4. Black FO, Pesznecker S, Stallings V (2004) Permanent gentamicin vestibulotoxicity. Otol Neurotol 25:559–569
5. Mamoto Y, Yamamoto K, Imai T, Tamura M, Kubo T (2002) Three-dimensional analysis of human locomotion in normal subjects and patients with vestibular deficiency. Acta Oto-Laryngol 122:495–500
6. Rinne T, Bronstein AM, Rudge P, Gresty MA, Luxon LM (1998) Bilateral loss of vestibular function: clinical findings in 53 patients. J Neurol 245:314–321
7. Della Santina CC, Migliaccio AA, Hayden R, Melvin T, Fridman GY, Chiang B, Davidovics NS, Dai C, Carey JP, Minor LB, Anderson I, Park H, Lyford-Pike S, Tang S (2010) Current and future management of bilateral loss of vestibular sensation - an update on the Johns Hopkins multichannel vestibular prosthesis project. Cochlear Implants Int 11:2–11
8. Living without a balancing mechanism (1952) N Engl J Med. https://doi.org/10.1056/NEJM195203202461207
9. Gillespie MB, Minor LB (1999) Prognosis in bilateral vestibular hypofunction. Laryngoscope 109:35–41
10. Lucieer F, Vonk P, Guinand N, Stokroos R, Kingma H, van de Berg R (2016) Bilateral vestibular hypofunction: insights in etiologies, clinical subtypes, and diagnostics. Front Neurol 7:26. https://doi.org/10.3389/fneur.2016.00026
11. Guinand N, Boselie F, Guyot J, Kingma H (2012) Quality of life of patients with bilateral vestibulopathy. Ann Otol Rhinol Laryngol 121:471–477
12. Grunbauer WM, Dieterich M, Brandt T (1998) Bilateral vestibular failure impairs visual motion perception even with the head still. Neuroreport 9:1807–1810
13. Stultiens JJA, Lewis RF, Phillips JO, Boutabla A, Della Santina CC, Glueckert R, van de Berg R (2023) The next challenges of vestibular implantation in humans. J Assoc Res Otolaryngol 24:401–412
14. Boutros PJ, Schoo DP, Rahman M, Valentin NS, Chow MR, Ayiotis AI, Morris BJ, Hofner A, Rascon AM, Marx A, Deas R, Fridman GY, Davidovics NS, Ward BK, Trevino C, Bowditch SP, Roberts DC, Lane KE, Gimmon Y, Schubert MC, Carey JP, Jaeger A, Della Santina CC (2019) Continuous vestibular implant stimulation partially restores eye-stabilizing reflexes. JCI Insight. https://doi.org/10.1172/jci.insight.128397
15. Schoo DP, Ayiotis AI, Brillet CF, Chow MR, Lane KE, Ward BK, Carey JP, Della Santina CC (2023) Vestibular implantation can work even after more than 20 years of bilateral vestibular hypofunction. Otol Neurotol 44:168–171
16. Chow MR, Ayiotis AI, Schoo DP, Gimmon Y, Lane KE, Morris BJ, Rahman MA, Valentin NS, Boutros PJ, Bowditch SP, Ward BK, Sun DQ, Treviño Guajardo C, Schubert MC, Carey JP, Della Santina CC (2021) Posture, gait, quality of life, and hearing with a vestibular implant. N Engl J Med 384:521–532
17. Sun DQ, Lehar M, Dai C, Swarthout L, Lauer AM, Carey JP, Mitchell DE, Cullen KE, Della Santina CC (2015) Histopathologic changes of the inner ear in rhesus monkeys after intratympanic gentamicin injection and vestibular prosthesis electrode array implantation. J Assoc Res Otolaryngol. https://doi.org/10.1007/s10162-015-0515-y
18. Hedjoudje A, Hayden R, Dai C, Ahn J, Rahman M, Risi F, Zhang J, Mori S, Della Santina CC (2019) Virtual rhesus labyrinth model predicts responses to electrical stimulation delivered by a vestibular prosthesis. J Assoc Res Otolaryngol. https://doi.org/10.1007/s10162-019-00725-3
19. Hedjoudje A, Schoo DP, Ward BK, Carey JP, Della Santina CC, Pearl M (2021) Vestibular implant imaging. AJNR Am J Neuroradiol. https://doi.org/10.3174/ajnr.A6991
20. Schoo DP, Ward BK, Chow MR, Ayiotis AI, Brillet CF, Boutros PJ, Lane KE, Lee CN, Morris BJ, Carey JP, Della Santina CC (2024) Vestibular implant surgery. Laryngoscope 134:1842–1846. https://doi.org/10.1002/lary.31004
21. Phillips JO, Ling L, Nie K, Jameyson E, Phillips CM, Nowack AL, Golub JS, Rubinstein JT (2015) Vestibular implantation and longitudinal electrical stimulation of the semicircular canal afferents in human subjects. J Neurophysiol 113:3866–3892
22. Hageman KN, Kalayjian ZK, Tejada F, Chiang B, Rahman MA, Fridman GY, Dai C, Pouliquen PO, Georgiou J, Della Santina CC, Andreou AG (2016) A CMOS neural interface for a multichannel vestibular prosthesis. IEEE Trans Biomed Circuits Syst. https://doi.org/10.1109/TBCAS.2015.2409797
23. Sluydts M, Curthoys I, Vanspauwen R, Papsin BC, Cushing SL, Ramos A, de Ramos Miguel A, Borkoski Barreiro S, Barbara M, Manrique M, Zarowski A (2020) Electrical vestibular stimulation in humans: a narrative review. Audiol Neurootol 25(1–2):6–24. https://doi.org/10.1159/000502407
24. Hayden R, Sawyer S, Frey E, Mori S, Migliaccio AA, Della Santina CC (2011) Virtual labyrinth model of vestibular afferent excitation via implanted electrodes: validation and application to design of a multichannel vestibular prosthesis. Exp Brain Res 210:623–640
25. D'Alessandro S, Handler M, Saba R, Garnham C, Baumgarten D (2022) Computer simulation of the electrical stimulation of the human vestibular system: effects of the reactive component of impedance on voltage waveform and nerve selectivity. J Assoc Res Otolaryngol 23:815–833
26. Migliaccio AA, Schubert MC, Jiradejvong P, Lasker DM, Clendaniel RA, Minor LB (2004) The three-dimensional vestibulo-ocular reflex evoked by high-acceleration rotations in the squirrel monkey. Exp Brain Res 159:433–446
27. Davidovics NS, Rahman MA, Dai C, Ahn J, Fridman GY, Della Santina CC (2013) Multichannel vestibular prosthesis employing modulation of pulse rate and current with alignment precompensation elicits improved VOR performance in monkeys. J Assoc Res Otolaryngol. https://doi.org/10.1007/s10162-013-0370-7

28. Dai C, Fridman GY, Chiang B, Rahman MA, Ahn JH, Davidovics NS, Della Santina CC (2013) Directional plasticity rapidly improves 3D vestibulo-ocular reflex alignment in monkeys using a multichannel vestibular prosthesis. J Assoc Res Otolaryngol. https://doi.org/10.1007/s10162-013-0413-0
29. Dai C, Fridman GY, Davidovics NS, Chiang B, Ahn JH, Della Santina CC (2011) Restoration of 3D vestibular sensation in rhesus monkeys using a multichannel vestibular prosthesis. Hear Res 281:74–83
30. Association for the Advancement of Medical Instrumentation (2017). ANSI/AAMI CI86:2017 Cochlear implant systems: requirements for safety, functional verification, labeling and reliability reporting. American National Standards Institute (ANSI), Arlington
31. Wobbrock JO, Findlater L, Gergle D, Higgins JJ (2011) The aligned rank transform for nonparametric factorial analyses using only ANOVA procedures. In: Proceedings of the SIGCHI Conference on Human Factors in Computing Systems (CHI '11). Association for Computing Machinery, New York, pp 143–146. https://doi.org/10.1145/1978942.1978963
32. Salter KC, Fawcett RF (1993) The art test of interaction: a robust and powerful rank test of interaction in factorial models. Commun Stat Simul Comput. https://doi.org/10.1080/03610919308813085
33. Bolker BM, Brooks ME, Clark CJ, Geange SW, Poulsen JR, Stevens MHH, White JS (2009) Generalized linear mixed models: a practical guide for ecology and evolution. Trends Ecol Evol. https://doi.org/10.1016/j.tree.2008.10.008
34. Della Santina CC, Potyagaylo V, Migliaccio AA, Minor LB, Carey JP (2005) Orientation of human semicircular canals measured by three-dimensional multiplanar CT reconstruction. J Assoc Res Otolaryngol. https://doi.org/10.1007/s10162-005-0003-x
35. Phillips C, Defrancisci C, Ling L, Nie K, Nowack A, Phillips JO, Rubinstein JT (2013) Postural responses to electrical stimulation of the vestibular end organs in human subjects. Exp Brain Res 229:181–195
36. Rubinstein JT, Bierer S, Kaneko C, Ling L, Nie K, Oxford T, Newlands S, Santos F, Risi F, Abbas PJ, Phillips JO (2012) Implantation of the semicircular canals with preservation of hearing and rotational sensitivity: a vestibular neurostimulator suitable for clinical research. Otol Neurotol 33:789–796
37. Guinand N, de Van Berg R, Cavuscens S, Stokroos RJ, Ranieri M, Pelizzone M, Kingma H, Guyot J, Perez-Fornos A (2015) Vestibular implants: 8 years of experience with electrical stimulation of the vestibular nerve in 11 patients with bilateral vestibular loss. ORL 77:227–240
38. Fornos AP, Guinand N, van de Berg R, Stokroos R, Micera S, Kingma H, Pelizzone M, Guyot J (2014) Artificial balance: restoration of the vestibulo-ocular reflex in humans with a prototype vestibular neuroprosthesis. Front Neurol 5:66
39. Wall C 3, Kos MI, Guyot J (2007) Eye movements in response to electric stimulation of the human posterior ampullary nerve. Ann Otol Rhinol Laryngol 116:369–374
40. Hageman KN, Chow MR, Roberts D, Boutros PJ, Tooker A, Lee K, Felix S, Pannu SS, Haque R, Della Santina CC (2020) Binocular 3D otolith-ocular reflexes: responses of chinchillas to prosthetic electrical stimulation targeting the utricle and saccule. J Neurophysiol 123:259–276
41. Macias AR, de Miguel AR, Montesdeoca IR, Barreiro SB, González JCF (2020) Chronic electrical stimulation of the otolith organ: preliminary results in humans with bilateral vestibulopathy and sensorineural hearing loss. Audiol Neurotol 25:79–90
42. Wang H, Northrop C, Burgess B, Liberman MC, Merchant SN (2006) Three-dimensional virtual model of the human temporal bone: a stand-alone, downloadable teaching tool. Otol Neurotol 27:452–457
43. Stultiens JJA, Postma AA, Guinand N, Perez Fornos A, Kingma H, van de Berg R (2020) Vestibular implantation and the feasibility of fluoroscopy-guided electrode insertion. Otolaryngol Clin North Am 53(1):115–126
44. Nie K, Bierer SM, Ling L, Oxford T, Rubinstein JT, Phillips JO (2011) Characterization of the electrically evoked compound action potential of the vestibular nerve. Otol Neurotol 32:88–97
45. Creighton FX, Unberath M, Song T, Zhao Z, Armand M, Carey J (2020) Early feasibility studies of augmented reality navigation for lateral skull base surgery. Otol Neurotol. https://doi.org/10.1097/MAO.0000000000002724
46. El Chemaly T, Athayde Neves C, Leuze C, Hargreaves B, H Blevins N (2023) Stereoscopic calibration for augmented reality visualization in microscopic surgery. Int J Comput Assist Radiol Surg. https://doi.org/10.1007/s11548-023-02980-5
47. Hussain R, Guigou C, Lalande A, Bozorg Grayeli A (2022) Vision-based augmented reality system for middle ear surgery: evaluation in operating room environment. Otol Neurotol. https://doi.org/10.1097/MAO.0000000000003441
48. Hussain R, Lalande A, Berihu Girum K, Guigou C, Grayeli AB (2020) Augmented reality for inner ear procedures: visualization of the cochlear central axis in microscopic videos. Int J Comput Assist Radiol Surg. https://doi.org/10.1007/s11548-020-02240-w
49. Neves CA, Tran ED, Kessler IM, Blevins NH (2021) Fully automated preoperative segmentation of temporal bone structures from clinical CT scans. Sci Rep. https://doi.org/10.1038/s41598-020-80619-0
50. Stypulkowski PH, van den Honert C (1984) Physiological properties of the electrically stimulated auditory nerve. I. Compound action potential recordings. Hear Res 14(3):205–223. https://doi.org/10.1016/0378-5955(84)90051-0
51. Brown CJ, Abbas PJ, Gantz B (1990) Electrically evoked whole-nerve action potentials: data from human cochlear implant users. J Acoust Soc Am 88:1385–1391
52. Jeng F, Abbas PJ, Brown CJ, Miller CA, Nourski KV, Robinson BK (2007) Electrically evoked auditory steady-state responses in Guinea pigs. Audiol Neuro-Otol 12:101–112
53. Nagel D (1974) Compound action potential of the cochlear nerve evoked electrically. Electrophysiological study of the acoustic nerve (guinea pig). Arch Otorhinolaryngol 206:293–298
54. Matsuoka AJ, Abbas PJ, Rubinstein JT, Miller CA (2000) The neuronal response to electrical constant-amplitude pulse train stimulation: evoked compound action potential recordings. Hear Res 149:115–128
55. Abbas PJ, Brown CJ, Shallop JK, Firszt JB, Hughes ML, Hong SH, Staller SJ (1999) Summary of results using the nucleus CI24M implant to record the electrically evoked compound action potential. Ear Hear 20:45–59
56. Brown CJ, Abbas PJ (1990) Electrically evoked whole-nerve action potentials: parametric data from the cat. J Acoust Soc Am 88:2205–2210
57. Brown CJ, Abbas PJ, Gantz BJ (1998) Preliminary experience with neural response telemetry in the nucleus CI24M cochlear implant. Am J Otol 19:320–327
58. Gantz BJ, Brown CJ, Abbas PJ (1994) Intraoperative measures of electrically evoked auditory nerve compound action potential. Am J Otol 15:137–144